SIAM J. APPL. MATH.
Vol. 78, No. 6, pp. 3213–3237
© 2018 Society for Industrial and Applied Mathematics

Downloaded 05/30/19 to 150.135.174.98. Redistribution subject to SIAM license or copyright; see http://www.siam.org/journals/ojsa.php

TRAVELING STRIPES IN THE KLAUSMEIER MODEL OF VEGETATION PATTERN FORMATION*

PAUL CARTER† AND ARJEN DOELMAN‡

Abstract. The Klausmeier equation is a widely studied reaction-diffusion-advection model of vegetation pattern formation on gently sloped terrain in semiarid ecosystems. We consider the case of constantly sloped terrain and study the formation of planar vegetation stripe patterns which align in the direction transverse to the slope and travel uphill. These patterns arise as solutions to an underlying traveling wave equation, which admits a separation of scales due to the fact that water flows downhill faster than the rate at which vegetation diffuses. We rigorously construct solutions corresponding to single vegetation stripes as well as long wavelength spatially periodic wave trains using geometric singular perturbation theory. Blow-up desingularization methods are needed to understand slow passage of solutions near a degenerate transcritical bifurcation. The underlying geometry of the traveling wave equation predicts relations between pattern wavelength, speed, and terrain slope.

Key words. pattern formation, reaction diffusion advection equations, geometric singular perturbation theory, blow-up desingularization, traveling waves

AMS subject classifications. 35K57, 35C07, 35B25, 34C25, 34C37, 35B36, 92D40

DOI. 10.1137/18M1196996

1. Introduction.

Vegetation patterns are pervasive in water limited regions [17, 22, 31, 33, 34, 44, 45], and it has been observed that on sloped terrain vegetation aligns in resilient striped patterns [1, 2, 8, 30, 42] due to an oriented flow of water downslope. The formation of such patterns is frequently modeled by reaction-diffusion equations, where an advective term accounts for downhill flow of water. One of the simplest and most commonly used models for studying vegetation patterns on sloped terrain is the Klausmeier model [22], a two-component reaction-diffusion-advection partial differential equation describing the evolution of water and plant biomass.

When suitably nondimensionalized, the model takes the form

$$\begin{aligned} U_t &= A - U - UV^2 + \frac{1}{\varepsilon}U_x, \\ V_t &= \Delta V - mV + UV^2, \end{aligned} \tag{1.1}$$

where $A, m > 0$ and $\Delta = \partial_{xx} + \partial_{yy}$. The components U, V represent water and plant biomass, respectively. The input parameter A represents rainfall, and the parameter m denotes the death rate of vegetation. The linear term $-U$ represents evaporation and the nonlinear term UV^2 represents water uptake by plants. This nonlinear term also appears in the second equation, where it represents plant growth. That is, the water consumption by vegetation converted into plant biomass at a constant rate. The two-dimensional terrain has constant slope, oriented so that "uphill" corresponds to direction of increasing x. The parameter $0 < \varepsilon \ll 1$ is taken small, which ensures that

*Received by the editors June 27, 2018; accepted for publication (in revised form) October 8, 2018; published electronically November 29, 2018.
http://www.siam.org/journals/siap/78-6/M119699.html
Funding: The first author's work was supported by NSF grant DMS–1815315.
†Department of Mathematics, University of Arizona, Tucson, AZ 85721 (pacarter@math.arizona.edu).
‡Mathematisch Instituut, Universiteit Leiden, Niels Bohrweg 1, 2333CA Leiden, Netherlands (doelman@math.leidenuniv.nl).

Copyright © by SIAM. Unauthorized reproduction of this article is prohibited.

Downloaded 05/30/19 to 150.135.174.98. Redistribution subject to SIAM license or copyright; see http://www.siam.org/journals/ojsa.php

the downhill advection term is large. This is not due to the steepness of the slope (such slopes are typically gentle) but rather reflects the separation of scales between the downhill flow of water versus the diffusion of plant biomass. The parameter values suggested by Klausmeier in [22] are $A = 0.94 - 2.81, m = 0.45$ for grass and $A = 0.077 - 0.23, m = 0.045$ for trees, with $\varepsilon = 0.005$.

Equation (1.1) admits a spatially homogeneous steady state

$$(U, V)(x, y, t) = (U_*, V_*) = (A, 0), \tag{1.2}$$

which corresponds to the bare desert state. In the case $A > 2m$, there also exist two other uniform steady states,

$$(U_\pm, V_\pm) = \left(\frac{A \pm \sqrt{A^2 - 4m^2}}{2}, \frac{A \mp \sqrt{A^2 - 4m^2}}{2m} \right). \tag{1.3}$$

Given the dominating appearance and resilience of striped patterns on hillsides with sufficiently steep slopes [1, 2, 8, 30, 42], we are interested in the (mathematical) formation of traveling vegetation stripe solutions. Such solutions are given as profiles $(U, V)(x, y, t) = (U, V)(x - St)$ which are constant in the direction transverse to the slope (the y-direction), and traveling toward increasing x, corresponding to positive wave speed $S > 0$. As is usual in the analysis of reaction-diffusion(-advection) equations, we first focus on the construction of localized patterns or pulses, i.e., patches of vegetation localized in the direction of slope and bordered on each side by the bare desert state (U_*, V_*). Figure 1 shows the U and V profiles of a localized stripe solution obtained by direct numerical simulation in (1.1) for the parameter values $A = 1.2, m = 0.45, \varepsilon = 0.005$. Also shown is a space-time plot of the location of the vegetation patch; note that the direction of motion is toward increasing x, corresponding to the uphill direction.

The behavior of stripe solutions to (1.1) has been studied in previous works, notably a collection of articles [36, 37, 38, 39, 40] in which the author investigates pattern solutions of (1.1) in various parameter regimes. However, results in the direction of far-from-onset or large amplitude patterns for (1.1) are primarily numerical or rely on formal leading order asymptotic analysis, and there is a notable lack of rigorous mathematical existence analysis. From the analytical point of view, much is known regarding pulse solutions in Gray–Scott type models [10, 11, 13, 20, 23, 24, 32] and in the so-called generalized Klausmeier–Gray–Scott model [35, 41, 43] in the context of vegetation pattern formation. The latter was originally proposed in [43] as a natural generalization of (1.1) in which the water component U also diffuses, typically

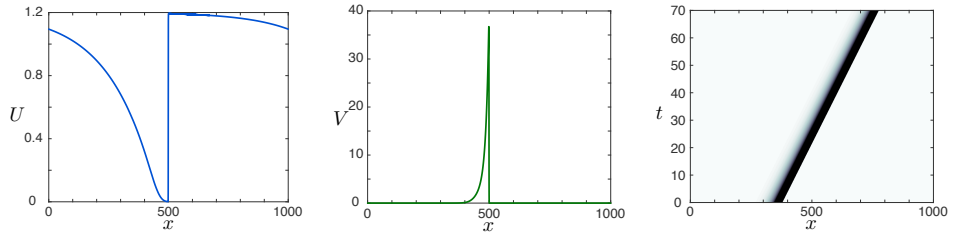

FIG. 1. *Shown are the U and V profiles (left and middle panels, respectively) of a traveling pulse solution of* (1.1) *obtained by direct numerical simulation with $A = 1.2$, $m = 0.45$, and $\varepsilon = 0.005$. The right panel depicts a space-time plot of the V-profile; the pulse travels to the right, corresponding to the uphill direction.*

Copyright © by SIAM. Unauthorized reproduction of this article is prohibited.

Downloaded 05/30/19 to 150.135.174.98. Redistribution subject to SIAM license or copyright; see http://www.siam.org/journals/ojsa.php

at a faster rate than that of the vegetation component. By stretching the classical methods originally introduced in [10, 11] to their limits, stripe solutions were constructed for the Klausmeier–Gray–Scott model in [35] for parameter values up to a certain maximal ratio between the advective and diffusive (water) transport effects. However, it was also shown in [35] that these stripe solutions must be unstable (with respect to transverse instabilities). Nevertheless, the simulations of [41] indicate that stripes may be stable beyond the region for which the methods of [35] apply, i.e., in cases where the advective effects are so strong that the ratio between the advective and diffusive effects passes beyond the (theoretical) upper bound of [35]. Note that the stabilizing effect of sloped terrain on vegetation stripes is in line with observations of real vegetation patterns [8, 9]. From this point of view, (1.1) arises as a natural "advection-dominant" limit, in which the diffusion of water is ignored entirely and the advection is assumed large, and serves as a first step in understanding the potentially stabilizing effect of downhill advection of water.

We therefore focus on (1.1) and aim to construct stripe solutions analytically. Motivated by Klausmeier's choice of parameters, we focus on the regime where the system parameters satisfy $0 < \varepsilon \ll 1$ and $0 < A, m = \mathcal{O}(1)$. In this regime, we construct traveling stripe solutions rigorously, using the methods of geometric singular perturbation theory [14] and blow-up desingularization [27, 28, 29]. In particular, we are able to construct (homoclinic) traveling pulse solutions, representing single vegetation stripes. Based on these insights, we next consider the ecologically more relevant spatially periodic vegetation patterns (see Figure 2) and establish the existence of a family of such traveling wave trains. All of these solutions travel in the uphill direction. While a stability analysis is outside the scope of this article, we do confirm that these solutions lie outside the geometric framework of those which fall into the two-dimensional–unstable regime in Klausmeier–Gray–Scott type models; in particular, the unstable Klausmeier–Gray–Scott pulses of [35] center around a fast homoclinic orbit that drives the transverse instability of the stripe, while the pulses constructed here are based on a fast heteroclinic jump.

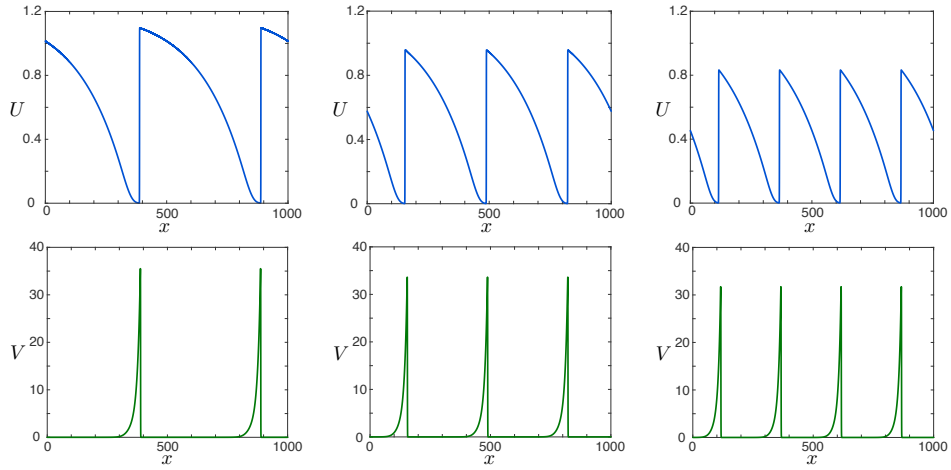

FIG. 2. *Depicted are the U and V profiles (upper and lower panels, respectively) of three traveling wave train solutions to* (1.1) *obtained via direct numerical simulations for values of $A = 1.2$, $m = 0.45$, and $\varepsilon = 0.005$. The spatial domain length is fixed at $L = 1000$ with periodic boundary conditions. Note that longer wavelength correlates with larger amplitude.*

Copyright © by SIAM. Unauthorized reproduction of this article is prohibited.

Downloaded 05/30/19 to 150.135.174.98. Redistribution subject to SIAM license or copyright; see http://www.siam.org/journals/ojsa.php

Concerning the existence of pulses, we have the following.

THEOREM 1.1. *There exists a unique $\theta_0 > 0$ such that the following holds. Fix $A, m > 0$. Then for all sufficiently small $\varepsilon > 0$, the Klausmeier equation* (1.1) *admits a traveling pulse solution $(U,V)(x,y,t) = (U,V)(x - St)$ with wave speed $S = (\frac{A^2\theta_0^2}{\varepsilon})^{1/3} + \mathcal{O}(1)$.*

The background of the crucial constant θ_0 will be discussed in the upcoming description of the singular nature of these orbits. Based on this result we establish the existence of (one-parameter families of) periodically repeating vegetation stripe pattern solutions.

THEOREM 1.2. *Fix $A, m > 0$ and $\Delta > 0$ sufficiently small. For all sufficiently small $\varepsilon > 0$, the Klausmeier equation* (1.1) *admits a family of traveling wave trains*

$$(U,V)(x,y,t) = (U,V)(x - S(k,\varepsilon)t; k, \varepsilon), \qquad k \in (\Delta, A), \tag{1.4}$$

with wave speeds $S(k,\varepsilon) = (\frac{k^2\theta_0^2}{\varepsilon})^{1/3} + \mathcal{O}(1)$, with θ_0 as in Theorem 1.1*, and amplitudes*

$$U_{\max}(k,\varepsilon) := \sup_{\xi \in [0, T(k,\varepsilon)]} |U(\xi; k, \varepsilon)| = k + h(k,\varepsilon), \tag{1.5}$$

where $|h(k,\varepsilon)| \to 0$ as $\varepsilon \to 0$, and the periods $T(k,\varepsilon) \to \infty$ as $\varepsilon \to 0$ for each fixed $k \in (\Delta, A)$. Furthermore, for each sufficiently small fixed ε, the periods $T(k,\varepsilon)$ satisfy $T(k,\varepsilon) \to \infty$ as $k \to A$, and the periodic orbits limit onto the pulse solution from Theorem 1.1*.*

From Theorems 1.1–1.2, we immediately obtain relations between properties of the emergent pattern solutions. First we note that the leading order expressions for the wave speeds in both theorems imply that the vegetation patches move uphill, which is in line with the (idealized) ecological mechanism which suggests that vegetation travels in the direction of the source of water. While this agrees with many observations, static vegetation stripe patterns have also been observed on slopes [4, 8]. Also, Theorems 1.1–1.2 predict that stripes travel faster for larger values of the slope, which is in line with prior results [36]. Although this is confirmed by the recent observations in [4], empirical data again paints a mixed picture [42], with some observations of negative correlation between speed and slope [16]. We further note that Theorem 1.2 predicts that longer wavelengths correspond to larger amplitudes (see Figure 2), which is confirmed by observations [4, 8]. Moreover, it should be remarked that the results of Theorems 1.1–1.2 concern "perfect" spatially periodic patterns on terrains with a "perfect" constant slope. It is shown in [3] (in the context of the generalized Klausmeier–Gray–Scott model) that pulses may indeed move downhill, due either to a change in slope or to the presence of other—nonequidistant—pulses. Nevertheless, there is a remarkable variability in relations between properties of empirical observations of vegetation patterns, and a highly simplified model such as (1.1) may not be capable of capturing all ecologically relevant behavior.

Our results on the existence of traveling wave solutions of (1.1) are established through the corresponding traveling wave equation

$$\begin{aligned} 0 &= \left(\frac{1}{\varepsilon} + S\right) U_\xi + A - U - UV^2, \\ 0 &= V_{\xi\xi} + SV_\xi - mV + UV^2, \end{aligned} \tag{1.6}$$

Copyright © by SIAM. Unauthorized reproduction of this article is prohibited.

Downloaded 05/30/19 to 150.135.174.98. Redistribution subject to SIAM license or copyright; see http://www.siam.org/journals/ojsa.php

obtained by substituting the ansatz $(U,V)(x,y,t) = (U,V)(x-St)$ into (1.1), where we have denoted the traveling wave variable by $\xi = x - St$. The existence analysis therefore reduces to understanding the dynamics of the three-dimensional ordinary differential equation (1.6), where we exploit the small parameter ε as a singular perturbation parameter. The existence of singular pulse (Theorem 1.1) and spatially periodic (Theorem 1.2) pattern solutions corresponds directly to similar results obtained in [35, 41] in the context of the generalized Klausmeier–Gray–Scott model, where the effect of water diffusion is included. In that case, the traveling wave existence problem is four-dimensional and the approach of [35, 41] runs along the lines of the literature on Gray–Scott type models. However, we emphasize that this approach does not extend to the present original Klausmeier equation (1.1)—see especially [35]. In each case the vegetation stripe patterns can be constructed as solutions of an associated traveling wave ODE, though the underlying geometry of this ODE changes when the diffusion of water is added. In particular, the construction of the pulse and/or periodic solutions in the Gray–Scott variety of models is based on the family of integrable homoclinic orbits of the planar fast reduced V-subsystem $V_{\xi\xi} - mV + \bar{U}V^2 = 0$ (cf. (1.6) with $S = 0$ and $U \equiv \bar{U}$) that governs the excursion of the full homoclinic/periodic orbit away from and back to a two-dimensional slow manifold. The present case differs essentially from this setting: the natural homoclinic orbit of the fast reduced V-subsystem does not play a role here (see also Remark 1.3).

The traveling pulse and wave train solutions of Theorems 1.1 and 1.2 correspond to singular orbits that can be seen as the (singular) compositions of three parts: a superslow part that follows a slow manifold that is not normally hyperbolic, a slow part along a standard normally hyperbolic manifold, and a fast jump along a planar heteroclinic connection. Similarly to the construction of traveling pulses in FitzHugh–Nagumo type equations [21], the fast jump determines the speed, and thus the crucial constant θ_0 that appears in both theorems. However, unlike these more classical models, the fast jump is described by a somewhat nonstandard planar system,

$$Z'' + \left(\theta - \frac{1}{\theta}Z^2\right)Z' + (1-Z)Z^2 = 0. \tag{1.7}$$

This system has two critical points: $(Z,Z') = (0,0)$ is degenerate and corresponds to the nonhyperbolic slow manifold, while the saddle $(Z,Z') = (1,0)$ represents the normally hyperbolic manifold. Apart from the eigenvalue $\lambda = 0$, $(0,0)$ also has a stable eigenvalue $\lambda = -\theta$ with an associated well-defined one-dimensional strong stable manifold $W^{ss}((0,0))$: θ_0 is defined as the unique value of θ for which $W^{ss}((0,0))$ coincides (partly) with the one-dimensional unstable manifold $W^u((1,0))$ of the saddle $(1,0)$—see section 2.2. The core of this paper is dedicated to the validation of this construction for $\varepsilon > 0$ (and sufficiently small). Very different from the classical four-dimensional Gray–Scott type existence problems, a central role is played by the geometric blow-up techniques as developed in [27, 28, 29]. Especially since the orbits we consider here must remain close to a nonhyperbolic slow manifold for "long times," the analytic construction is quite subtle.

The remainder of this paper is organized as follows. In section 2, we study (1.6) as a slow-fast system in the context of geometric singular perturbation theory, and we construct singular homoclinic and periodic orbits. The persistence of these solutions for small $\epsilon > 0$ and the proofs of Theorems 1.1 and 1.2 will be given in section 3. We conclude with results of numerical simulations and a brief discussion in section 4.

Copyright © by SIAM. Unauthorized reproduction of this article is prohibited.

Remark 1.3. It is possible to construct homoclinic and periodic solutions of (1.6) that do follow a fast reduced limit homoclinic solution of $V_{\xi\xi} - mV + \bar{U}V^2 = 0$ in the fast field. However, the U-components of these patterns necessarily must remain asymptotically close to $U^* = A$, the U-component of the trivial desert state (1.2). As a consequence, these patterns are both ecologically unrealistic and unstable as solutions of (1.1).

2. Slow-fast analysis. We rewrite the traveling wave equation (1.6) as a first order equation

$$\begin{aligned} U_\xi &= \frac{\varepsilon}{1+\varepsilon S}\left(U - A + UV^2\right), \\ V_\xi &= Q, \\ Q_\xi &= mV - UV^2 - SQ. \end{aligned} \tag{2.1}$$

The disparity between the amplitudes of the U and V profiles in the results of numerical simulations (see Figures 1 and 2) motivates a rescaling of the variables. We perform the rescaling

$$S = \frac{s}{\varepsilon^{1/3}}, \quad U = u, \quad V = \frac{v}{s\varepsilon^{2/3}}, \quad Q = \frac{q}{\varepsilon}, \quad \xi = \varepsilon^{1/3}s^2\tau, \quad \delta = s\varepsilon^{2/3}, \tag{2.2}$$

which results in the rescaled traveling wave equation

$$\begin{aligned} \dot{u} &= \frac{1}{1+\delta}\left(uv^2 + \delta^2(u - A)\right), \\ \dot{v} &= s^3 q, \\ \dot{q} &= \delta m v - uv^2 - s^3 q, \end{aligned} \tag{2.3}$$

where $\dot{} = \frac{d}{d\tau}$. Stripe patterns manifest as periodic orbits, or homoclinic orbits to the equilibrium $(u, v, q) = (A, 0, 0)$ representing the spatially homogeneous desert state solution $(U_*, V_*) = (A, 0)$ of (1.1). The rescaled equation (2.3) has lost the slow-fast structure of the original equation (2.1). However, there is also a slow-fast separation in (2.3), which can be seen by defining the new variable

$$w = (1+\delta)u + v + q,$$

whereby (2.3) becomes

$$\begin{aligned} \dot{w} &= \delta m v + \frac{\delta^2}{1+\delta}\left(w - v - q - a\right), \\ \dot{v} &= s^3 q, \\ \dot{q} &= \delta m v - \frac{1}{1+\delta}(w - v - q)v^2 - s^3 q, \end{aligned} \tag{2.4}$$

where we have set $a = (1+\delta)A$. We refer to the traveling wave equation (2.4) as the "fast" system, and in the new variables, we search for orbits homoclinic to the equilibrium $(w, v, q) = (a, 0, 0)$.

The strategy for constructing the solutions outlined in Theorems 1.1 and 1.2 is to exploit the slow-fast separation in the traveling wave equation (2.4) which arises due to the presence of the small parameter $0 < \delta \ll 1$. The goal of this section is to construct singular orbits for $\delta = 0$ which will persist for small $\delta > 0$ as solutions of the full traveling wave equation (2.4). These singular solutions will be composed of

Copyright © by SIAM. Unauthorized reproduction of this article is prohibited.

Downloaded 05/30/19 to 150.135.174.98. Redistribution subject to SIAM license or copyright; see http://www.siam.org/journals/ojsa.php

Downloaded 05/30/19 to 150.135.174.98. Redistribution subject to SIAM license or copyright; see http://www.siam.org/journals/ojsa.php

concatenated portions of critical manifolds, which manifest as manifolds of equilibria of the system (2.4) when $\delta = 0$, with fast jumps along heteroclinic orbits in the associated layer problem. The critical manifolds and their associated reduced flows are described in section 2.1, followed by a description of the layer problem in section 2.2. Finally in section 2.3, we construct singular $\delta = 0$ homoclinic and periodic orbits which will serve as the basis for the stripe solutions of Theorems 1.1 and 1.2. The persistence of these solutions for small $\delta > 0$ will be proved in section 3.

Remark 2.1. We assumed that parameters A and m of (1.1) are of $\mathcal{O}(1)$ with respect to the small parameter ε. Like in [35], in which traveling waves in the generalized Klausmeier–Gray–Scott model are studied, one could perform a more general scaling analysis. The outcome of such an analysis is a system very much like (2.4); the only essential difference is that the δ^2 factor in the w-equation of (2.4) will be replaced by a factor δ^χ for some (free) parameter $\chi > 0$. For $\chi \leq 1$ this yields several other types of solutions. Such (ecologically relevant) orbits are also considered in work in progress in the context of a modified version of (1.1) [2]; we refrain from going into this issue here.

2.1. The critical manifolds $\mathcal{M}_0^{\ell/r}$. By setting $\delta = 0$ in the fast system (2.4) we obtain the planar layer problem

$$\begin{aligned} \dot{v} &= s^3 q, \\ \dot{q} &= -(w - v - q)v^2 - s^3 q, \end{aligned} \tag{2.5}$$

parameterized by w. There are two equilibria $p_1(w)$ and $p_2(w)$ given by $(v, q) = (0, 0)$ and $(v, q) = (w, 0)$, respectively, which coincide for $w = 0$. The equilibrium $p_2(w)$ is a hyperbolic saddle for each $w > 0$, while $p_1(w)$ is nonhyperbolic with one negative and one zero eigenvalue. Therefore, the set of equilibria $\mathcal{M}_0^r = \{p_2(w) : w \in \mathbb{R}\}$ forms a critical manifold which is normally hyperbolic for $w > 0$, while the set $\mathcal{M}_0^\ell = \{p_1(w) : w \in \mathbb{R}\}$ forms a manifold of nonhyperbolic equilibria. These two manifolds intersect at the origin in a manner which can be described as a degenerate transcritical bifurcation.

For $w_m, w_M \in \mathbb{R}$ with $w_m < w_M$, we will use the notation

$$\begin{aligned} \mathcal{M}_0^\ell(w_m, w_M) &= \{p_1(w) : w \in [w_m, w_M]\}, \\ \mathcal{M}_0^r(w_m, w_M) &= \{p_2(w) : w \in [w_m, w_M]\} \end{aligned} \tag{2.6}$$

to refer to subsets of the critical manifolds $\mathcal{M}_0^{\ell/r}$.

We now determine the reduced flow on each of the critical manifolds $\mathcal{M}_0^{\ell/r}$. For $\mathcal{M}_0^r$, we rescale $\sigma = \delta\tau$ in (2.4) and obtain the slow system

$$\begin{aligned} w_\sigma &= mv + \frac{\delta}{1+\delta}\left(w - v - q - a\right), \\ \delta v_\sigma &= s^3 q, \\ \delta q_\sigma &= \delta m v - \frac{1}{1+\delta}(w - v - q)v^2 - s^3 q, \end{aligned} \tag{2.7}$$

and upon setting $\delta = 0$ we obtain the reduced problem

$$\begin{aligned} w_\sigma &= mv, \\ 0 &= s^3 q, \\ 0 &= -(w - v - q)v^2 - s^3 q. \end{aligned} \tag{2.8}$$

Copyright © by SIAM. Unauthorized reproduction of this article is prohibited.

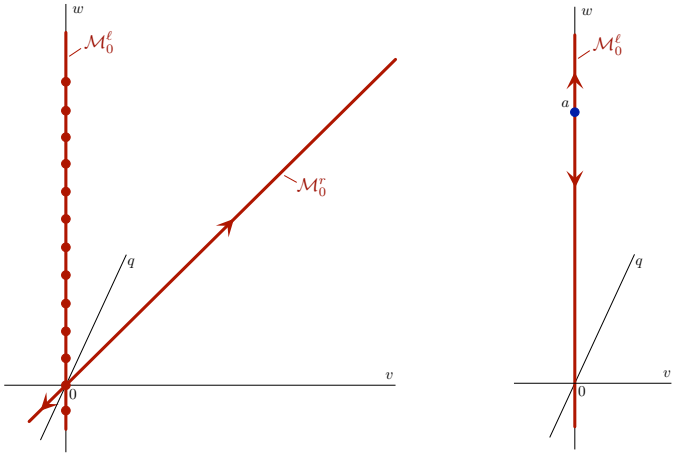

FIG. 3. *Shown are dynamics on the critical manifolds $\mathcal{M}_0^{\ell/r}$ within the slow (left) and superslow (right) reduced systems.*

Here the flow is restricted to the union $\mathcal{M}_0^r \cup \mathcal{M}_0^\ell$, and within $\mathcal{M}_0^r$, the dynamics are governed by the single equation

$$w_\sigma = mw, \tag{2.9}$$

which admits an unstable equilibrium at $w = 0$. Within the reduced system (2.8), $\mathcal{M}_0^\ell$ consists of equilibria; see Figure 3, left panel.

To determine the flow on $\mathcal{M}_0^\ell$, we note that $\mathcal{M}_0^\ell$ is an invariant set for all δ. Returning to the system (2.4), and considering the flow on $\mathcal{M}_0^\ell$ on the "superslow" timescale $\zeta = \delta^2\tau$, we obtain the reduced equation

$$w_\zeta = w - a, \tag{2.10}$$

which admits a single repelling equilibrium at $w = a$; see Figure 3, right panel.

2.2. Layer problem: Singular fronts. In this section, we study fast connections between the manifolds $\mathcal{M}_0^{\ell/r}$. We recall that for each w, the layer equation (2.5) admits two equilibria $p_1(w), p_2(w)$, which coincide for $w = 0$. The critical manifold $\mathcal{M}_0^r = \{p_2(w) : w \in \mathbb{R}\}$ is normally hyperbolic for $w > 0$, while $\mathcal{M}_0^\ell = \{p_1(w) : w \in \mathbb{R}\}$ forms a manifold of nonhyperbolic equilibria. The manifolds formed by the union of the stable/unstable manifolds of the equilibria $p_2(w)$ for $w > 0$ form two-dimensional (un)stable manifolds $\mathcal{W}^s(\mathcal{M}_0^r), \mathcal{W}^u(\mathcal{M}_0^r)$ of the normally hyperbolic critical manifold $\mathcal{M}_0^r$.

Within the layer problem (2.5), the equilibrium $p_1(w)$ has a unique strong stable manifold $\mathcal{W}^{ss}(p_1(w))$, and we are interested in heteroclinic orbits between $p_2(w)$ and $p_1(w)$ which approach $p_1(w)$ along $\mathcal{W}^{ss}(p_1(w))$. We note that the equilibrium $(a, 0, 0)$ of the full system (2.4), which corresponds to the spatially homogeneous desert state solution, coincides with $p_1(a)$. We have the following (see Figure 4).

PROPOSITION 2.2. *Consider* (2.5) *for $w > 0$. There exists a unique $s = s^*(w) > 0$ such that there is a heteroclinic orbit from $p_2(w)$ to $p_1(w)$, which we denote by $\phi_{\mathrm{f}}(w)$, which approaches $p_1(w)$ along the strong stable manifold $\mathcal{W}^{ss}(p_1(w))$.*

Downloaded 05/30/19 to 150.135.174.98. Redistribution subject to SIAM license or copyright; see http://www.siam.org/journals/ojsa.php

Copyright © by SIAM. Unauthorized reproduction of this article is prohibited.

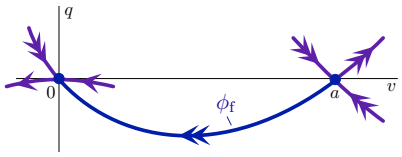

FIG. 4. *Shown is the geometry of the layer problem* (2.5) *for* $w = a$*, along with the heteroclinic connection* $\phi_f(a)$*, which exists for* $s = s^*(a)$.

Proof. We begin by proving that there is some value of $s = s^*(w)$ for which the orbit $\phi_f(w)$ exists. We consider the planar system (2.5) for fixed $w > 0$,

$$\begin{aligned} \dot{v} &= s^3 q, \\ \dot{q} &= -(w - v - q)v^2 - s^3 q. \end{aligned} \tag{2.11}$$

We track the behavior of $\mathcal{W}^{ss}(p_1(w))$ under the backward flow of (2.11) as s varies. The linearization of (2.11) about $p_1(w)$ has eigenvalues $0, -s^3$ with corresponding eigenvectors $(1, 0)$ and $(1, -1)$, respectively. In particular, this means that the manifold $\mathcal{W}^{ss}(p_1(w))$ approaches $p_1(w)$ asymptotically along the line $q = -v$. We are concerned with the branch of $\mathcal{W}^{ss}(p_1(w))$ which approaches $p_1(w)$ via the region $q < 0 < v$.

We note that along the curve $v + q = 0$, we have $\dot{v} + \dot{q} < 0$ when $v > 0$. Further, along the line $v = w$, we have $\dot{v} < 0$ when $v > 0$. Finally, along the curve $q = 0$ we have $\dot{v} = 0$ and $\dot{q} < 0$ for $0 < v < w$. In particular, this means that in backward time, $\mathcal{W}^{ss}(p_1(w))$ enters the triangular region $\mathcal{T}$ bounded by the curves $q = -v, v = w$, and $q = 0$ and has one of three possible fates: $\mathcal{W}^{ss}(p_1(w))$ can exit this region via the boundaries $B_1 = \{q = 0, v < w\}$ or $B_2 = \{v = w, q < 0\}$ or must converge to the equilibrium $p_2(w) = (w, 0)$.

We further note that the line $v + q = w$ is invariant under the flow of (2.11). In particular, if $\mathcal{W}^{ss}(p_1(w))$ enters the region $q > 0$ via the boundary B_1 in backward time, then $\mathcal{W}^{ss}(p_1(w))$ is confined to the region $0 < q < w - v$ for all (backward) time. Similarly, if $\mathcal{W}^{ss}(p_1(w))$ enters the region $v > w$ via the boundary B_2 in backward time, then $\mathcal{W}^{ss}(p_1(w))$ is confined to the region $0 < q < w - v$ for all (backward) time. That is, once $\mathcal{W}^{ss}(p_1(w))$ leaves $\mathcal{T}$ via either of these boundaries in backward time, $\mathcal{W}^{ss}(p_1(w))$ never returns to $\mathcal{T}$.

We proceed via a continuity argument for each $w > 0$. We show that for small values of the speed s, $\mathcal{W}^{ss}(p_1(w))$ leaves $\mathcal{T}$ via B_1 in backward time, while for large values of s, $\mathcal{W}^{ss}(p_1(w))$ leaves $\mathcal{T}$ via B_2, which implies the existence of a speed $s = s^*(w)$ for which $\mathcal{W}^{ss}(p_1(w))$ must connect to the equilibrium $p_2(w)$.

Within $\mathcal{T}$, we note that

$$\frac{dq}{dv} = -\frac{(w - v - q)v^2}{s^3 q} - 1 \tag{2.12}$$

and since $w - v - q > -q$ in $\mathcal{T}$, we have

$$\frac{dq}{dv} > \frac{v^2}{s^3} - 1, \tag{2.13}$$

from which we deduce that $\mathcal{W}^{ss}(p_1(w))$ lies above the curve $q = \frac{v^3}{3s^3} - v$ within $\mathcal{T}$. By taking $s^3 < w^2/3$, we ensure that $\mathcal{W}^{ss}(p_1(w))$ must exit $\mathcal{T}$ via B_1.

Copyright © by SIAM. Unauthorized reproduction of this article is prohibited.

Downloaded 05/30/19 to 150.135.174.98. Redistribution subject to SIAM license or copyright; see http://www.siam.org/journals/ojsa.php

Downloaded 05/30/19 to 150.135.174.98. Redistribution subject to SIAM license or copyright; see http://www.siam.org/journals/ojsa.php

On the other hand, whenever $q < -2wv^2/s^3$ and $s^3 > 2w^2$, within $\mathcal{T}$ we have that

$$\frac{(w-q)v^2}{-s^3 q} < 1 \tag{2.14}$$

and thus

$$\frac{dq}{dv} < \frac{v^3}{s^3 q}. \tag{2.15}$$

We deduce that $\mathcal{W}^{ss}(p_1(w))$ lies below the curve $q = -v^2/\sqrt{2s^3}$ within $\mathcal{T}$ whenever $q < -2wv^2/s^3$. In particular, this means that in backward time $\mathcal{W}^{ss}(p_1(w))$ must exit $\mathcal{T}$ via the boundary B_2 whenever $s^3 > 8w^2$.

Therefore, there exists a heteroclinic connection between the equilibria $p_2(w)$ and $p_1(w)$ which approaches $p_1(w)$ along $\mathcal{W}^{ss}(p_1(w))$ for some value $s = s^*(w)$ which satisfies $w^2/3 < s^*(w)^3 < 8w^2$.

Finally, we consider the uniqueness of $s^*(w)$. We consider (2.11) and compute the distance between $\mathcal{W}^u(p_2(w))$ and $\mathcal{W}^{ss}(p_1(w))$ to first order in $s - s^*(w)$. We consider the adjoint equation of the linearization of (2.11) about the front ϕ_{f} given by

$$\dot{\psi} = \begin{pmatrix} 0 & -(3v_{\mathrm{f}}(\tau)^2 - 2wv_{\mathrm{f}}(\tau) + 2v_{\mathrm{f}}(\tau)q_{\mathrm{f}}(\tau)) \\ -s^*(w)^3 & s^*(w)^3 - v_{\mathrm{f}}(\tau)^2 \end{pmatrix} \psi. \tag{2.16}$$

The space of solutions which grow as $\tau \to \infty$ at most algebraically is one-dimensional and spanned by

$$\psi_{\mathrm{f}}(\tau) := e^{s^*(w)^3\tau - \int_0^\tau v_{\mathrm{f}}(\zeta)^2 d\zeta} \begin{pmatrix} -q_{\mathrm{f}}'(\tau) \\ v_{\mathrm{f}}'(\tau) \end{pmatrix}. \tag{2.17}$$

Let F_0 denote the right-hand side of (2.11). Then the Melnikov integral

$$\begin{aligned} M_s &= \int_{-\infty}^{\infty} D_s F_0(\phi_{\mathrm{f}}(\tau)) \cdot \psi_{\mathrm{f}}(\tau) d\tau \\ &= 3s^*(w)^2 \int_{-\infty}^{\infty} e^{s^*(w)^3\tau - \int_0^\tau v_{\mathrm{f}}(\zeta)^2 d\zeta} (w - v_{\mathrm{f}}(\tau) - q_{\mathrm{f}}(\tau)) v_{\mathrm{f}}(\tau)^2 q_{\mathrm{f}}(\tau) d\tau \\ &< 0 \end{aligned}$$

measures the splitting of $\mathcal{W}^u(p_2(w))$ and $\mathcal{W}^{ss}(p_1(w))$ along ϕ_{f} to first order in $s - s^*(w)$. In particular, this guarantees the local uniqueness of the heteroclinic connection $\phi_{\mathrm{f}}(w)$. As the sign of the Melnikov coefficient is fixed independent of $s^*(w)$, this also guarantees the uniqueness of the heteroclinic orbit over all values of s. ∎

Remark 2.3. We note that there can be additional heteroclinic connections between the equilibria $p_1(w), p_2(w)$ which approach $p_1(w)$ along a weak center direction for other values of s. However, we will see in section 3 that in the full system for $\delta > 0$, any such orbits are blocked from approaching the manifold $\mathcal{M}_0^\ell$ and are not relevant in the construction of traveling pulses and wave trains.

From the Melnikov analysis in the proof of Proposition 2.2, we immediately obtain the following.

Copyright © by SIAM. Unauthorized reproduction of this article is prohibited.

Downloaded 05/30/19 to 150.135.174.98. Redistribution subject to SIAM license or copyright; see http://www.siam.org/journals/ojsa.php

COROLLARY 2.4. *For each $w > 0$, the intersection of the manifolds $\mathcal{W}^u(\mathcal{M}_0^r)$ and $\mathcal{W}^{ss}(p_1(w))$ along the singular front $\phi_{\mathrm{f}}(w)$ is transverse in s, and the splitting function*

$$D_0(s;w) = M_s(w)(s - s^*(w)) + \mathcal{O}(|s - s^*(w)|^2) \tag{2.18}$$

measures the distance between $\mathcal{W}^u(\mathcal{M}_0^r)$ and $\mathcal{W}^{ss}(p_1(w))$ for $s \approx s^*(w)$.

We now introduce Z, Q, η, and θ by the rescalings

$$v = wZ, \quad q = wQ, \quad \tau = \frac{\eta}{w^2\theta}, \quad s = w^{2/3}\theta^{2/3}, \tag{2.19}$$

which results in

$$\begin{aligned} \frac{dZ}{d\eta} &= \theta Q, \\ \frac{dQ}{d\eta} &= \frac{1}{\theta}\left[-(1 - Z - Q)Z^2 - \theta^2 Q\right], \end{aligned} \tag{2.20}$$

which coincides with planar system (1.7). Moreover, by construction, $s^*(w)$ as introduced in Proposition 2.2 corresponds to θ_0 as defined in Theorems 1.1 and 1.2 through $s^*(w) = w^{2/3}\theta_0^{2/3}$ so that indeed (by Proposition 2.2) θ_0 is the value of θ for which a connection between $W^{ss}((0,0))$ and $W^u((1,0))$ exists in (1.7) or equivalently (2.20).

Remark 2.5. By the above analysis, we have that $\frac{1}{3}\sqrt{3} < \theta_0 < 2\sqrt{2}$. Numerically, we can approximate the value of θ_0, and we determine that critical speed $s = s^*(w)$ for which the front ϕ_{f} exists is given by $s^*(w) = w^{2/3}\theta_0^{2/3}$, where $\theta_0 \approx 0.8615$.

2.3. Singular traveling wave solutions. From the analysis of the reduced/layer problems in sections 2.1–2.2, we are able to define singular homoclinic orbits and periodic orbits for the system (2.4).

We first construct a singular homoclinic orbit, or traveling pulse solution, as follows. There is a singular trajectory which first departs the equilibrium $p_1(a)$ along the critical manifold $\mathcal{M}_0^\ell$ in the superslow timescale, and upon reaching $w = 0$ then transitions to $\mathcal{M}_0^r$ in the slow timescale. By concatenating this trajectory with the singular front $\phi_{\mathrm{f}}(a)$, we obtain a singular homoclinic orbit

$$\mathcal{H}_0 = \mathcal{M}_0^\ell(0,a) \cup \mathcal{M}_0^r(0,a) \cup \phi_{\mathrm{f}}(a) \tag{2.21}$$

to the equilibrium $p_1(a)$; see Figure 5.

For periodic orbits, the construction is similar. For each value of $k \in (\Delta, a)$, there exists a singular periodic orbit

$$\mathcal{P}_0(k) = \mathcal{M}_0^\ell(0,k) \cup \mathcal{M}_0^r(0,k) \cup \phi_{\mathrm{f}}(k) \tag{2.22}$$

obtained by first following the portion of the critical $\mathcal{M}_0^\ell$ in the region $w \in [0,k]$, then following the critical manifold $\mathcal{M}_0^r$ in the slow timescale from $w = 0$ to the plane $w = k$, and finally returning to $\mathcal{M}_0^\ell$ along the singular front $\phi_{\mathrm{f}}(k)$ which exists for $s = s^*(k)$.

3. Persistence of solutions for $0 < \delta \ll 1$. In this section, we construct solutions for sufficiently small $\delta > 0$ based on the singular solutions described in section 2.3 and complete the proofs of the main existence Theorems 1.1 and 1.2. Much of the analysis involved is related to studying the flow in neighborhoods of the critical manifolds $\mathcal{M}_0^{\ell/r}$ for small $\delta > 0$. In section 3.1, we analyze the flow near $\mathcal{M}_0^\ell$ and in particular study the behavior of the unstable manifold $\mathcal{W}^u(p_1(a))$ of the

Copyright © by SIAM. Unauthorized reproduction of this article is prohibited.

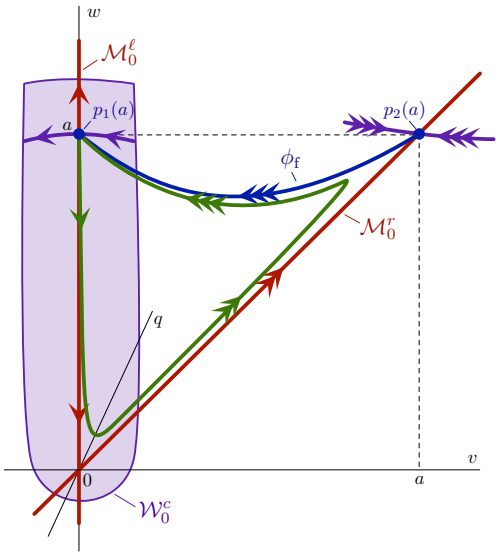

FIG. 5. *Shown is the geometry of the singular pulse solution* $\mathcal{H}_0$.

equilibrium $p_1(a)$. The flow near $\mathcal{M}_0^\ell$ is analyzed in section 3.2, followed by the proofs of Theorems 1.1 and 1.2, which are given in sections 3.3 and 3.4, respectively.

3.1. The flow near $\mathcal{M}_0^\ell$ for $0 < \delta \ll 1$. The flow near $\mathcal{M}_0^\ell$ requires care as this manifold is not normally hyperbolic, so standard methods of geometric singular perturbation theory do not apply. The equilibria $p_1(w)$ which comprise $\mathcal{M}_0^\ell$ are nonhyperbolic with one center direction and one strong stable direction. We therefore begin by constructing a two-dimensional normally attracting center manifold $\mathcal{W}_0^c$ which contains $\mathcal{M}_0^\ell$.

We consider a compact segment of $\mathcal{M}_0^\ell$ which contains the equilibria $p_1(w)$ for $-\rho \le w \le a + \rho$, that is, a connected segment of $\mathcal{M}_0^\ell$ which includes both the origin and the equilibrium $p_1(a)$ of the full system (2.4). We consider the linearization of (2.5) about $p_1(w)$, which has eigenvalues $\lambda_1^0 = 0$ and $\lambda_1^- = -s^3$ and associated eigenvectors

$$e_1^0 = \begin{pmatrix} 1 \\ 0 \end{pmatrix}, \quad e_1^- = \begin{pmatrix} 1 \\ -1 \end{pmatrix}. \tag{3.1}$$

Therefore, for $\delta = 0$, these equilibria all have one center direction and one stable direction which depend smoothly on w. Therefore, by the center manifold theorem, in a neighborhood of each equilibrium $p_1(w)$, there exists a center manifold which depends C^k-smoothly on w, which can be represented as a graph over the center eigenspace. The union of all these center manifolds for $-\rho \le w \le a + \rho$ forms a C^k-smooth normally attracting invariant manifold $\mathcal{W}_0^c$ which contains $\mathcal{M}_0^\ell$.

This manifold therefore persists as a two-dimensional locally invariant C^k-smooth normally attracting manifold $\mathcal{W}_\delta^c$ for $0 < \delta \ll 1$. We now determine the flow on $\mathcal{W}_\delta^c$. We begin by straightening the center/stable eigenspaces by defining the variable $z = v + q$, whence (2.4) becomes

Copyright © by SIAM. Unauthorized reproduction of this article is prohibited.

Downloaded 05/30/19 to 150.135.174.98. Redistribution subject to SIAM license or copyright; see http://www.siam.org/journals/ojsa.php

$$\begin{aligned}\dot{w} &= \delta m(z-q) + \frac{\delta^2}{1+\delta}\left(w - z - a\right),\\ \dot{z} &= \delta m(z-q) - \frac{1}{1+\delta}(w-z)(z-q)^2,\\ \dot{q} &= \delta m(z-q) - \frac{1}{1+\delta}(w-z)(z-q)^2 - s^3 q.\end{aligned} \tag{3.2}$$

The center manifold $\mathcal{W}^c_\delta$ is given as a graph $q = f(w, z, \delta)$. Since $\mathcal{W}^c_\delta$ contains the invariant set $\{z = q = 0\}$, we have that $f(w, z, \delta) = \mathcal{O}(\delta z, z^2)$. Defining $\tilde{q} = q - f(w, z, \delta)$, we obtain

$$\begin{aligned}\dot{w} &= \delta m(z - \tilde{q} - f(w,z,\delta)) + \frac{\delta^2}{1+\delta}\left(w - z - a\right),\\ \dot{z} &= \delta m(z - \tilde{q} - f(w,z,\delta)) - \frac{1}{1+\delta}(w-z)\left(z - \tilde{q} - f(w,z,\delta)\right)^2,\\ \dot{\tilde{q}} &= \left(-s^3 + h(w,z,\tilde{q},\delta)\right)\tilde{q},\end{aligned} \tag{3.3}$$

where $h(w, z, \tilde{q}, \delta) = \mathcal{O}(z, \tilde{q}, \delta)$, whence the flow on $\mathcal{W}^c_\delta$ is determined by $\tilde{q} = 0$. By performing a final coordinate change to straighten out the strong stable fibers, we obtain

$$\begin{aligned}\dot{w} &= \delta m(z - f(w,z,\delta)) + \frac{\delta^2}{1+\delta}\left(w - z - a\right),\\ \dot{z} &= \delta m(z - f(w,z,\delta)) - \frac{1}{1+\delta}(w-z)\left(z - f(w,z,\delta)\right)^2,\\ \dot{\tilde{q}} &= \left(-s^3 + \tilde{h}(w,z,\tilde{q},\delta)\right)\tilde{q},\end{aligned} \tag{3.4}$$

by a slight abuse of notation again denoted in terms of $(w, z, \tilde{q})$ and where again $\tilde{h}(w, z, \tilde{q}, \delta) = \mathcal{O}(z, \tilde{q}, \delta)$. Hence we have decomposed the flow into the two-dimensional dynamics of basepoints on $\mathcal{W}^c_\delta$ and the flow along the one-dimensional strong stable fibers. We now focus on the flow of basepoints on the center manifold $\mathcal{W}^c_\delta$, determined by

$$\begin{aligned}\dot{w} &= \delta m z(1 + \mathcal{O}(\delta, z)) + \frac{\delta^2}{1+\delta}\left(w - z - a\right),\\ \dot{z} &= \delta m z\left(1 + \mathcal{O}(\delta, z)\right) - \frac{1}{1+\delta}(w-z)z^2\left(1 + \mathcal{O}(\delta, z)\right).\end{aligned} \tag{3.5}$$

We break the analysis into four regions $R_1 - R_4$, which require different scalings. The first region R_1 determines the flow near $\mathcal{M}^\ell_0$ for $z = \mathcal{O}(\delta)$. The regions R_2, R_3 concern the transition from $z = \mathcal{O}(\delta)$ to $(w, z) = \mathcal{O}(\delta^{1/2})$, and the final region R_4 determines how the dynamics for $(w, z) = \mathcal{O}(\delta^{1/2})$ match up with the normally hyperbolic manifold $\mathcal{M}^r_\delta$ in the region $(w, z) = \mathcal{O}(1)$.

3.1.1. The region R_1. We begin with the region $z = \mathcal{O}(\delta)$, which will allow us to determine the local stable/unstable manifolds of the equilibrium $p_1(a)$ for $\delta > 0$. We rescale $z = \delta z_1$, whence we obtain

$$\begin{aligned}\dot{w} &= \delta^2 m z_1(1 + \mathcal{O}(\delta)) + \frac{\delta^2}{1+\delta}\left(w - \delta z_1 - a\right),\\ \dot{z_1} &= \delta m z_1\left(1 + \mathcal{O}(\delta)\right) - \frac{\delta}{1+\delta}(w - \delta z_1)z_1^2\left(1 + \mathcal{O}(\delta)\right).\end{aligned} \tag{3.6}$$

Downloaded 05/30/19 to 150.135.174.98. Redistribution subject to SIAM license or copyright; see http://www.siam.org/journals/ojsa.php

Copyright © by SIAM. Unauthorized reproduction of this article is prohibited.

Downloaded 05/30/19 to 150.135.174.98. Redistribution subject to SIAM license or copyright; see http://www.siam.org/journals/ojsa.php

On the slow timescale, we obtain

$$\begin{aligned} w' &= \delta m z_1(1+\mathcal{O}(\delta)) + \frac{\delta}{1+\delta}\left(w-\delta z_1 - a\right), \\ z_1' &= m z_1\left(1+\mathcal{O}(\delta)\right) - \frac{1}{1+\delta}(w-\delta z_1) z_1^2\left(1+\mathcal{O}(\delta)\right), \end{aligned} \tag{3.7}$$

which gives a new slow-fast system with respect to the "superslow" time $t_1 = \delta\sigma = \delta^2\tau$. Setting $\delta = 0$ in (3.7) gives the layer problem

$$\begin{aligned} w' &= 0, \\ z_1' &= m z_1 - w z_1^2, \end{aligned} \tag{3.8}$$

which has two hyperbolic equilibria $q_1(w), q_2(w)$ given by $z = 0$ and $z = \frac{m}{w}$, respectively, for each $w > 0$. The equilibrium $q_1(w)$ is repelling while $q_2(w)$ is attracting. Therefore, away from $w = 0$, there exist normally hyperbolic critical manifolds $\mathcal{C}_0^1$ and $\mathcal{C}_0^2$ formed by the sets of equilibria $\{q_1(w) : w \in \mathbb{R}\}$ and $\{q_2(w) : w \geq \rho\}$, respectively.

With respect to the superslow time t_1, we obtain the reduced systems on each of the critical manifolds $\mathcal{C}_0^1$ and $\mathcal{C}_0^2$. On $\mathcal{C}_0^1$, the reduced flow is given by

$$\frac{dw}{dt_1} = w - a, \tag{3.9}$$

while on $\mathcal{C}_0^2$, the reduced flow is

$$\frac{dw}{dt_1} = \frac{m^2}{w} + w - a. \tag{3.10}$$

We see that for $a < 2m$, there are no equilibria on $\mathcal{C}_0^2$, with a saddle-node bifurcation occurring when $a = 2m$, resulting in two equilibria given by

$$w_\pm = \frac{a \pm \sqrt{a^2 - 4m^2}}{2} \tag{3.11}$$

when $a > 2m$. The equilibrium at $w = w_-$ is attracting while that at $w = w_+$ is repelling.

The manifolds $\mathcal{C}_0^1$ and $\mathcal{C}_0^2$ perturb to one-dimensional locally invariant manifolds $\mathcal{C}_\delta^1$ and $\mathcal{C}_\delta^2$, on which the slow flow is an $\mathcal{O}(\delta)$ perturbation of the respective reduced flows (3.9) and (3.9). See Figure 6 for a schematic in each of the cases $a > 2m$ and $a < 2m$.

Furthermore the unstable manifold $\mathcal{W}^u(\mathcal{C}_0^1)$ of $\mathcal{C}_0^1$ and the stable manifold $\mathcal{W}^s(\mathcal{C}_0^2)$ of $\mathcal{C}_0^2$ persist as two-dimensional locally invariant manifolds $\mathcal{W}^u(\mathcal{C}_\delta^1)$ and $\mathcal{W}^s(\mathcal{C}_\delta^2)$. The equilibrium $p_1(a)$ of the full system (2.4) lies on $\mathcal{C}_\delta^1$ on which it is locally repelling within $\mathcal{W}_\delta^c$. In particular we now determine that for $0 < \delta \ll 1$, the equilibrium $p_1(a)$ becomes hyperbolic with two-dimensional unstable manifold $\mathcal{W}^u(p_1(a)) = \mathcal{W}^u(\mathcal{C}_\delta^1)$ and one-dimensional stable manifold given by the strong stable fiber $\mathcal{W}^{ss}(p_1(a))$ of $\mathcal{W}_\delta^c$ with basepoint at $p_1(a)$.

Additionally, for the case of $a > 2m$, the equilibria $w = w_\pm$ of the reduced system (3.10) persist as equilibria $p_\pm$ of the full system for $0 < \delta \ll 1$ and we immediately obtain the following.

PROPOSITION 3.1. *Fix $a, m > 0$ satisfying $a > 2m$. Then for all sufficiently small $\delta > 0$, there exists a unique front solution ϕ_+ between the equilibria $p_1(a)$ and p_+, and unique front solution ϕ_- between the equilibria $p_1(a)$ and p_- which approaches p_- along its strong stable manifold.*

Copyright © by SIAM. Unauthorized reproduction of this article is prohibited.

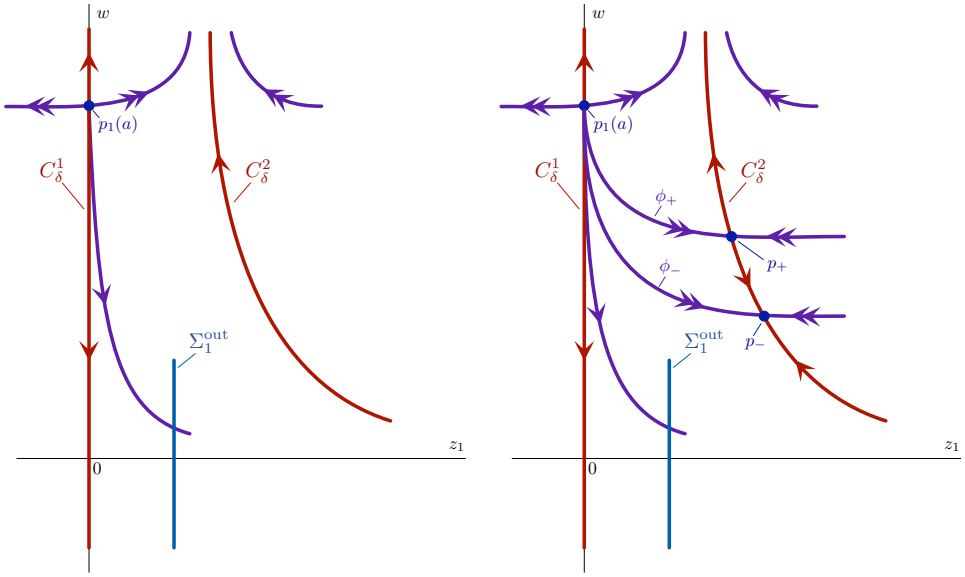

(a) $a < 2m$ (b) $a > 2m$

FIG. 6. *Shown are the dynamics of* (3.7) *in the region* R_1 *for* $0 < \delta \ll 1$ *in the cases* $a < 2m$ *(left panel) and* $a > 2m$ *(right panel). In the latter case, additional equilibria* $p_\pm$ *persist on the slow manifold* $\mathcal{C}^2_\delta$ *and there exist fronts* $\phi_\pm$ *which connect* $p_1(a)$ *to each of* $p_\pm$*, with* ϕ_- *approaching* p_- *along a strong stable manifold. In each case, we have that* $\Sigma_1^{\text{out}} \subset \mathcal{W}^u(p_1(a))$.

Proof. The result follows from geometric singular perturbation theory applied to the planar system (3.7). ∎

Remark 3.2. The equilibria $p_\pm$ correspond to the spatially homogeneous vegetated steady states $(U_\pm, V_\pm)$ of (1.1) defined in (1.3). Each of the front solutions $\phi_\pm$ therefore describes the invasion of the barren desert state into a uniformly vegetated state.

We now focus on tracking the unstable manifold $\mathcal{W}^u(p_1(a))$ through the region $w \approx 0$. In particular, for $|w|$ bounded, all points which lie in a small neighborhood of $\mathcal{C}^1_\delta$ lie on $\mathcal{W}^u(p_1(a))$. For $z_1 > 0$, we see from (3.6) that $z_1' > 0$; hence we may integrate forward and see that $\mathcal{W}^u(p_1(a))$ extends to $z_1 = 1/\mu$ for $\mu > 0$ independent of δ, provided δ is sufficiently small.

To summarize, we may therefore define the section $\Sigma_1^{\text{out}} = \{(w, z_1, \delta) : |w| \leq \delta^{1/2}/\mu, z_1 = 1/\mu, 0 \leq \delta \leq \kappa^2\mu^2\}$ for κ sufficiently small, which thus consists entirely of points which lie on $\mathcal{W}^u(p_1(a))$.

3.1.2. The regions R_2 and R_3. The region R_3 concerns the passage near $w, z = \mathcal{O}(\delta^{1/2})$. We therefore perform the rescaling $w = \delta_3 w_3, z = \delta_3 z_3, \delta = \delta_3^2$, which results in the system

$$\begin{aligned} \dot{w_3} &= \delta_3^2 m z_3 (1 + \mathcal{O}(\delta_3^2, \delta_3 z_3)) + \frac{\delta_3^3}{1+\delta_3^2} (\delta_3 w_3 - \delta_3 z_3 - a), \\ \dot{z_3} &= \delta_3^2 m z_3 \left(1 + \mathcal{O}(\delta_3^2, \delta_3 z_3)\right) - \frac{\delta_3^2}{1+\delta_3^2} (w_3 - z_3) z_3^2 \left(1 + \mathcal{O}(\delta_3^2, \delta_3 z_3)\right), \end{aligned} \tag{3.12}$$

Copyright © by SIAM. Unauthorized reproduction of this article is prohibited.

Downloaded 05/30/19 to 150.135.174.98. Redistribution subject to SIAM license or copyright; see http://www.siam.org/journals/ojsa.php

Downloaded 05/30/19 to 150.135.174.98. Redistribution subject to SIAM license or copyright; see http://www.siam.org/journals/ojsa.php

which on the slow timescale $\sigma = \delta\tau = \delta_3^2\tau$ results in

$$\begin{aligned} w_3' &= mz_3 + \mathcal{O}(\delta_3), \\ z_3' &= mz_3 + z_3^3 - w_3z_3^2 + \mathcal{O}(\delta_3^2 z_3, \delta_3 z_3^2). \end{aligned} \tag{3.13}$$

The region R_2 concerns the transition from R_1, where $z = \mathcal{O}(\delta)$, to R_3, where $z = \mathcal{O}(\delta^{1/2})$. We thus perform the secondary projective rescaling

$$\delta_3 = z_3\delta_2 \tag{3.14}$$

which is valid in the region $z_3 > 0$, which results in the system

$$\begin{aligned} w_3' &= mz_3(1 + \mathcal{O}(\delta_2)), \\ z_3' &= mz_3 + z_3^3 - w_3z_3^2 + \mathcal{O}(\delta_2^2 z_3^3, \delta_2 z_3^3), \\ \delta_2' &= -m\delta_2(1 + \mathcal{O}(\delta_2, z_3)). \end{aligned} \tag{3.15}$$

In the region $D_2 = \{(w_3, z_3, \delta_2) : |w_3| \le 3, 0 \le z_3 \le \rho, 0 \le \delta_2 \le \mu\}$, solutions are confined to curves which satisfy

$$\begin{aligned} \frac{dw_3}{dz_3} &= \frac{1 + \mathcal{O}(\delta_2)}{1 + \mathcal{O}(z_3^2, w_3z_3, \delta_2 z_3^2)} \\ &= 1 + \mathcal{O}(\delta_2, z_3). \end{aligned} \tag{3.16}$$

We define the entry/exit sections

$$\Sigma_2^{\text{in}} = D_2 \cap \{|w| \le 2, \delta_2 = \mu\}, \qquad \Sigma_2^{\text{out}} = D_2 \cap \{|w| \le 1, z_3 = \kappa\}. \tag{3.17}$$

Due to (3.16), a solution which enters D via Σ_2^{in} at a point $(w_3, z_3, \delta_2) = (w_{3,0}, z_{3,0}, \mu_2)$ remains on a curve which satisfies

$$w_3 = w_{3,0} + z_3(1 + \mathcal{O}(\mu, \kappa)), \tag{3.18}$$

throughout its passage through D_2, and hence must exit D_2 via the set $\{z_3 = \kappa\}$. This solution therefore exits D_2 at a point $(w_3, z_3, \delta_2) = (w_{3,1}, \rho, \delta_{2,1})$ where $w_{3,1} = w_{3,0} + \mathcal{O}(\kappa)$; that is, the w_3 coordinate of any solution entering D_2 via Σ_2^{in} changes by no more than $\mathcal{O}(\kappa)$ before exiting via the set $\{z_3 = \kappa\}$. In particular, this means that the section $\Sigma_2^{\text{in}} = D_2 \cap \{|w| \le 2, \delta_2 = \mu\}$ is mapped *onto* the section $\Sigma_2^{\text{out}} = D_2 \cap \{|w| \le 1, z_3 = \kappa\}$.

We now focus on the passage through R_3. Recalling the relation $\delta_3 = z_3\delta_2$, in the R_3 coordinates, the section Σ_2^{out} is given by

$$\Sigma_2^{\text{out}} = \Sigma_3^{\text{in}} = \{(w_3, z_3, \delta_3) : |w| \le 1, z_3 = \kappa, 0 \le \delta_3 \le \kappa\mu\}. \tag{3.19}$$

We consider the flow in R_3 for $\delta_3 = 0$, given by

$$\begin{aligned} w_3' &= mz_3, \\ z_3' &= mz_3 + z_3^3 - w_3z_3^2, \end{aligned} \tag{3.20}$$

and by defining the new variable $x_3 = z_3 - w_3$, we obtain the system

$$\begin{aligned} x_3' &= z_3^2 x_3, \\ z_3' &= mz_3 + z_3^2 x_3, \end{aligned} \tag{3.21}$$

which leaves the subspace $x_3 = 0$ invariant with flow given by $z_3' = mz_3$. The time spent between $z_3 = \kappa$ and $z_3 = 1/\mu$ for fixed $\mu, \kappa > 0$ is finite. We fix $\gamma > 0$ sufficiently small; then for all $\rho > 0$ small enough, by a regular perturbation we can ensure that under the flow of (3.13), the section Σ_3^{in} is mapped *onto* the section

$$\Sigma_3^{\text{out}} = \{(w_3, z_3, \delta_3) : |z_3 - w_3| \le \gamma, w_3 = 1/\mu, 0 \le \delta_3 \le \rho\mu\}. \tag{3.22}$$

Copyright © by SIAM. Unauthorized reproduction of this article is prohibited.

Downloaded 05/30/19 to 150.135.174.98. Redistribution subject to SIAM license or copyright; see http://www.siam.org/journals/ojsa.php

3.1.3. The region R_4: Blow-up rescaling near $\mathcal{M}_\delta^r$. We now study how solutions on the center manifold $\mathcal{W}_\delta^c$ behave near the critical manifold $\mathcal{M}_0^r$. We perform the projective rescaling

$$z = wz_4, \quad \delta = w^2\delta_4, \tag{3.23}$$

which is valid in the region $w > 0$. This results in the system

$$\begin{aligned} \dot{w} &= mw^3\delta_4(z_4 + \mathcal{O}(w)), \\ \dot{z_4} &= \frac{1}{1+\delta_4 w} w^2 z_4^2(z_4 - 1) + \mathcal{O}(\delta_4 w^2, w^3), \\ \dot{\delta_4} &= -2mw^2\delta_4^2(z_4 + \mathcal{O}(w)), \end{aligned} \tag{3.24}$$

which we desingularize by a rescaling of time $dt_4 = w^2 d\tau$ and obtain

$$\begin{aligned} \frac{dw}{dt_4} &= mw\delta_4(z_4 + \mathcal{O}(w)), \\ \frac{dz_4}{dt_4} &= z_4^2(z_4 - 1) + \mathcal{O}(\delta_4, w), \\ \frac{d\delta_4}{dt_4} &= -2m\delta_4^2(z_4 + \mathcal{O}(w)). \end{aligned} \tag{3.25}$$

The line $L_4 = \{\delta_4 = w = 0\}$ is invariant with dynamics

$$\frac{dz_4}{dt_4} = z_4^2(z_4 - 1) \tag{3.26}$$

and thus contains two equilibria, at $z_4 = 0$ and $z_4 = 1$, which we refer to as q_0, q_1, respectively (see Figure 7). The equilibrium q_1 at $z_4 = 1$ is hyperbolic repelling with respect to the reduced flow on L_4 with eigenvalue $\lambda_4 = 1$. The linearization of the full equation (3.25) additionally admits a double zero eigenvalue. The plane $\{\delta_4 = 0\}$ is also invariant with dynamics

$$\begin{aligned} \frac{dw}{dt_4} &= 0, \\ \frac{dz_4}{dt_4} &= z_4^2(z_4 - 1) + \mathcal{O}(w). \end{aligned} \tag{3.27}$$

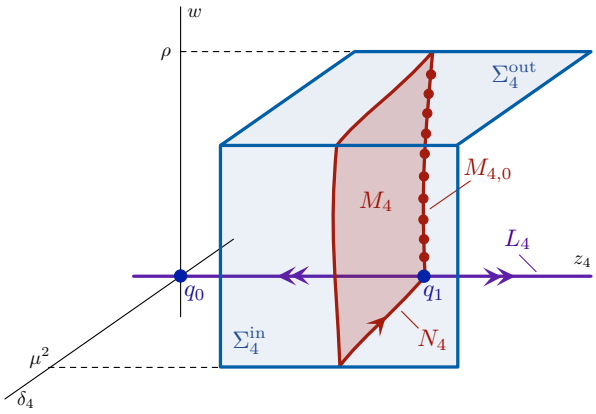

FIG. 7. *Shown are the dynamics of* (3.25) *in the region* R_4.

Copyright © by SIAM. Unauthorized reproduction of this article is prohibited.

Downloaded 05/30/19 to 150.135.174.98. Redistribution subject to SIAM license or copyright; see http://www.siam.org/journals/ojsa.php

This system has a normally hyperbolic curve of equilibria $M_{4,0} = \{z_4 = 1 + \mathcal{O}(w)\}$ which emanates from q_1 and exactly corresponds to the critical manifold $\mathcal{M}_0^r$ in the original coordinates. In the invariant plane $w = 0$, the dynamics are given by

$$\begin{aligned} \frac{dz_4}{dt_4} &= z_4^2(z_4 - 1) + \mathcal{O}(\delta_4), \\ \frac{d\delta_4}{dt_4} &= -2m\delta_4^2 z_4. \end{aligned} \tag{3.28}$$

Here we still have the equilibrium q_1 which has a zero eigenvalue due to the second equation, and hence there exists a one-dimensional center manifold N_4 at q_1 along which δ_4 decreases. Note that the branch of N_4 in the half space $\delta_4 > 0$ is unique.

For any sufficiently small $\beta, \rho, \mu > 0$, we restrict attention to the set

$$D_4 = \{(w, z_4, \delta_4) : 0 \le w \le \rho, |z_4 - 1| \le \beta, 0 \le \delta_4 \le \mu^2\}. \tag{3.29}$$

The next result follows from standard center manifold theory.

PROPOSITION 3.3. *For all sufficiently small $\beta, \rho, \mu > 0$, the following holds for the dynamics of* (3.25) *within D_4. There exists a repelling center manifold M_4 at q_1 which contains the line of equilibria $M_{4,0}$ and the center manifold N_4. In D_4, M_4 is given as a graph $z_4 = h_4(w, \delta_4) = -1 + \mathcal{O}(w, \delta_4)$. Furthermore, there exists an unstable invariant foliation with base M_4 and one-dimensional fibers.*

We define the following sections:

$$\Sigma_4^{\text{in}} = D_4 \cap \{\delta_4 = \mu^2\}, \qquad \Sigma_4^{\text{out}} = D_4 \cap \{w = \rho\}. \tag{3.30}$$

We note that in the R_4 coordinates, the section Σ_3^{out} is given by

$$\Sigma_3^{\text{out}} = \{(w, z_4, \delta_4) : 0 \le w \le \rho, |z_4 - 1| \le \gamma\mu, \delta_4 = \mu^2\} \subseteq \Sigma_4^{\text{in}}. \tag{3.31}$$

By setting $\beta = \gamma\mu$, we have that the flow of (3.25) maps Σ_4^{in} *onto* Σ_4^{out}, from which we deduce that Σ_4^{out} consists entirely of points on $\mathcal{W}^u(p_1(a))$.

Transforming to the original (w, z, δ) coordinates, we sum up the results of this section in the following.

PROPOSITION 3.4. *For each sufficiently small $\rho > 0$, there exists $\beta > 0$ such that the following holds. For all sufficiently small $\delta > 0$, within the center manifold $\mathcal{W}_\delta^c$, the set $\Sigma^{out} := \{(w, z) : w = \rho, |z - w| \le \beta\rho\}$ is contained in $\mathcal{W}^u(p_1(a))$.*

3.2. The flow near $\mathcal{M}_0^r$ for $0 < \delta \ll 1$. We now determine the reduced flow on the normally hyperbolic critical manifold $\mathcal{M}_0^r$. We rescale time by $\sigma = \delta\tau$ and obtain the slow system

$$\begin{aligned} w' &= mv + \frac{\delta}{1+\delta}(w - v - q - a), \\ \delta v' &= s^3 q, \\ \delta q' &= \delta m v - \frac{1}{1+\delta}(w - v - q)v^2 - s^3 q, \end{aligned} \tag{3.32}$$

where $' = \frac{d}{d\sigma}$, whence for $\delta = 0$ we determine the reduced flow restricted to $\mathcal{M}_0^r$ as

$$w' = mw. \tag{3.33}$$

Copyright © by SIAM. Unauthorized reproduction of this article is prohibited.

Downloaded 05/30/19 to 150.135.174.98. Redistribution subject to SIAM license or copyright; see http://www.siam.org/journals/ojsa.php

As the manifold $\mathcal{M}_0^r$ is normally hyperbolic for $w > 0$, using standard results of geometric singular perturbation theory, for $0 < \delta \ll 1$, $\mathcal{M}_0^r$ perturbs to a one-dimensional locally invariant manifold $\mathcal{M}_\delta^r$ which is C^1-$\mathcal{O}(\delta)$-close to $\mathcal{M}_0^r$, on which the flow is an $\mathcal{O}(\delta)$ perturbation of the reduced flow (2.8). Furthermore, in a neighborhood of $\mathcal{M}_0^r$, the stable/unstable manifolds $\mathcal{W}^s(\mathcal{M}_0^r), \mathcal{W}^u(\mathcal{M}_0^r)$ perturb to two-dimensional locally invariant manifolds $\mathcal{W}^s(\mathcal{M}_\delta^r), \mathcal{W}^u(\mathcal{M}_\delta^r)$ which are C^1-$\mathcal{O}(\delta)$-close to $\mathcal{W}^s(\mathcal{M}_0^r), \mathcal{W}^u(\mathcal{M}_0^r)$.

We now determine how the slow manifold $\mathcal{M}_\delta^r$ approaches $\mathcal{W}_\delta^c$ under the backward flow of (2.4). As $\mathcal{M}_\delta^r$ is normally hyperbolic in the region $w > 0$, we can track $\mathcal{M}_\delta^r$ until $w = \rho$. Further, from above we have that $\mathcal{M}_\delta^r$ is $\mathcal{O}(\delta)$-close to $\mathcal{M}_0^r$, which is given by the set of equilibria $\{p_2(w) : w \geq \rho\}$. Therefore $\mathcal{M}_\delta^r$ is $\mathcal{O}(\delta)$-close to the curve $\{v = w, q = 0\}$, and we have that the two-dimensional stable manifold $\mathcal{W}^s(\mathcal{M}_\delta^r)$ of $\mathcal{M}_\delta^r$ transversely intersects the two-dimensional center manifold $\mathcal{W}_\delta^c$ at $w = \rho$ at a point $(w, v, q) = (\rho, \rho + \mathcal{O}(\delta), \mathcal{O}(\delta))$. The results of Proposition 3.4 thus guarantee that for δ sufficiently small, $\mathcal{W}^s(\mathcal{M}_\delta^r)$ in fact transversely intersects $\mathcal{W}^u(p_1(a))$ in the set $\{w = \rho\}$.

Tracking $\mathcal{W}^u(p_1(a))$ forward under the flow of (2.4), by the exchange lemma $\mathcal{W}^u(p_1(a))$ aligns C^1-$\mathcal{O}(e^{-C/\delta})$-close to $\mathcal{W}^u(\mathcal{M}_\delta^r)$ (for some constant $C > 0$) upon exiting a neighborhood of $\mathcal{M}_\delta^r$.

3.3. Construction of pulses. In this section, we complete the proof of Theorem 1.1 by matching $\mathcal{W}^u(p_1(a))$ and $\mathcal{W}^{ss}(p_1(a))$.

Proof of Theorem 1.1. We compute the distance between $\mathcal{W}^u(p_1(a))$ and $\mathcal{W}^{ss}(p_1(a))$ along the singular front $\phi_{\mathrm{f}}(a)$. By the results of section 3.2, upon exiting a neighborhood of $\mathcal{M}_\delta^r$, $\mathcal{W}^u(p_1(a))$ aligns C^1-$\mathcal{O}(e^{-C/\delta})$-close to the manifold $\mathcal{W}^u(\mathcal{M}_\delta^r)$, which is itself a C^1-$\mathcal{O}(\delta)$ perturbation of $\mathcal{W}^s(\mathcal{M}_0^r)$.

Using Corollary 2.4, we can therefore compute the distance between $\mathcal{W}^u(p_1(a))$ and $\mathcal{W}^{ss}(p_1(a))$ to leading order in $\delta > 0$ and $s \approx s^*$ as

$$\begin{aligned} D(s,\delta) &= M_s(s - s^*(a)) + \mathcal{O}(\delta, e^{-C/\delta}, |s - s^*(a)|^2) \\ &= M_s(s - s^*(a)) + \mathcal{O}(\delta, |s - s^*(a)|^2), \end{aligned} \tag{3.34}$$

which can be solved for $D(s, \delta) = 0$ when $s = s^*(a) + \mathcal{O}(\delta)$ by the implicit function theorem. This corresponds to an intersection of $\mathcal{W}^u(p_1(a))$ and $\mathcal{W}^{ss}(p_1(a))$, and thus a homoclinic orbit in the traveling wave equation (2.4) which is $\mathcal{O}(\delta^{1/2})$-close to the singular orbit $\mathcal{H}_0$.

Using Proposition 2.2, noting $a = (1 + \delta)A$, and undoing the rescalings (2.2) and (2.19), we obtain the leading order expression

$$S = \left(\frac{A^2\theta_0^2}{\varepsilon}\right)^{1/3} + \mathcal{O}(1) \tag{3.35}$$

for the wave speed S of the pulse solution. ∎

3.4. Construction of periodic orbits. We now turn to the construction of periodic orbits and complete the proof of Theorem 1.2. The singular periodic orbits $\mathcal{P}_0(k)$ have similar geometry to the homoclinic orbit constructed in section 3.3, composed of portions of the critical manifolds $\mathcal{M}_0^{\ell/r}$ and a singular front $\phi_{\mathrm{f}}(k)$, and we will therefore be able to call on results from the pervious sections on properties of the flow near $\mathcal{M}_0^{\ell/r}$. The periodic orbits will then be obtained as fixed points of an appropriate Poincaré map.

Copyright © by SIAM. Unauthorized reproduction of this article is prohibited.

Downloaded 05/30/19 to 150.135.174.98. Redistribution subject to SIAM license or copyright; see http://www.siam.org/journals/ojsa.php

Proof of Theorem 1.2. We define a Poincaré section near $\mathcal{M}_0^\ell$ in the $(w, z, \tilde{q})$ coordinates from section 3.1. Recall that within this coordinate system, the center manifold $\mathcal{W}_\delta^c$ is given by the set $\{\tilde{q} = 0\}$, and the flow is decomposed into the two-dimensional dynamics of basepoints on $\mathcal{W}_\delta^c$ and the flow along one-dimensional strong stable fibers parametrized by $\tilde{q}$, given by the system

$$\begin{aligned} \dot{w} &= \delta m z(1 + \mathcal{O}(\delta, z)) + \frac{\delta^2}{1+\delta}(w - z - a), \\ \dot{z} &= \delta m z\,(1 + \mathcal{O}(\delta, z)) - \frac{1}{1+\delta}(w - z)z^2\,(1 + \mathcal{O}(\delta, z)), \\ \dot{\tilde{q}} &= \Big(-s^3 + \tilde{h}(w, z, \tilde{q}, \delta)\Big)\,\tilde{q}, \end{aligned} \tag{3.36}$$

where $\tilde{h}(w, z, \tilde{q}, \delta) = \mathcal{O}(z, \tilde{q}, \delta)$. In these coordinates, the equilibrium $p_1(a)$ is given by $(w, z, \tilde{q}) = (a, 0, 0)$, and for $\delta = 0$, the manifold $\mathcal{M}_0^\ell$ is given by the set $\{z = \tilde{q} = 0\}$.

We consider the flow of (3.36) in the set $\{(w, z, \tilde{q}\} : w \in [\Delta_w, a + \Delta_w], |z| \le \Delta_z, |\tilde{q}| \le \Delta_{\tilde{q}}\}$, and we place a two-dimensional section $\Sigma^{\mathrm{p}} = \{(w, z, \Delta_{\tilde{q}}\} : w \in [\Delta_w, a], |z| \le \Delta_z\}$ which will serve as the Poincaré section for the construction of periodic orbits. We denote the corresponding Poincaré map by $\Pi^{\mathrm{p}} : \Sigma^{\mathrm{p}} \to \Sigma^{\mathrm{p}}$.

For each $k \in [\Delta_w, a + \Delta_w]$, by Proposition 2.2, for $\delta = 0$, there exists a front $\phi_{\mathrm{f}}(k)$ which connects $\mathcal{M}_0^r$ and $\mathcal{M}_0^\ell$ in the plane $\{w = k\}$ when $s = s^*(k)$. In the local $(w, z, \tilde{q})$ coordinates, the front $\phi_{\mathrm{f}}(k)$ corresponds to the strong stable fiber $\{(k, 0, \tilde{q}) : q \in [0, \Delta_{\tilde{q}}]\}$ of the basepoint $(k, 0, 0)$; this basepoint corresponds to the equilibrium $p_1(k)$ of the layer problem (2.5) in the plane $\{w = k\}$. Within Σ^{p}, we can thus represent the manifold $\mathcal{M}_\delta^r$ as a graph over w,

$$\mathcal{M}_\delta^r \cap \Sigma^{\mathrm{p}} = \{(w, z, \Delta_{\tilde{q}}) : z = z^r(w; s, \delta)\}, \tag{3.37}$$

where z^r is a smooth function which satisfies $z^r(w; s^*(w), 0) = 0$ for each w.

For each $k \in [\Delta_w, a)$, we consider a small interval of initial conditions $\mathcal{I}(k) = \{(k, z, \Delta_{\tilde{q}}\} : |z| \le \Delta_z\}$ for Δ_z chosen sufficiently small. We consider the forward evolution of $\mathcal{I}(k)$ under the flow of (3.36), which traces out a two-dimensional manifold $\bar{\mathcal{I}}(k)$. By the analysis in sections 3.1.1–3.1.2 of the flow in the regions R_1, R_2 for $0 < \delta \ll 1$, it is apparent that a subset of $\bar{\mathcal{I}}(k)$ of width $\mathcal{O}(\delta)$ is quickly contracted to the unstable manifold $\mathcal{W}^u(p_1(a))$ and aligns C^1-$\mathcal{O}(e^{-C/\delta})$ close to $\mathcal{W}^u(p_1(a))$ upon entering the region R_2. Continuing to track $\bar{\mathcal{I}}(k)$ through the regions R_2–R_4, the C^1-$\mathcal{O}(e^{-C/\delta})$ closeness of $\bar{\mathcal{I}}(k)$ and $\mathcal{W}^u(p_1(a))$ guarantees that $\bar{\mathcal{I}}(k)$ transversely intersects $\mathcal{W}^s(\mathcal{M}_\delta^r)$. Thus by the exchange lemma $\bar{\mathcal{I}}(k)$ aligns C^1-$\mathcal{O}(e^{-C/\delta})$-close to $\mathcal{W}^u(\mathcal{M}_\delta^r)$ upon exiting a neighborhood of $\mathcal{M}_\delta^r$.

In particular, after this excursion, $\bar{\mathcal{I}}(k)$ again meets the section Σ^{p}, now in a curve $z = I^*(w; s, \delta, k)$ which satisfies $|z^r(w; s, \delta) - I^*(w; s, \delta, k)| = \mathcal{O}(e^{-C/\delta})$ for $|w - k| \le \Delta$ for $0 < \Delta \ll \Delta_w$ fixed sufficiently small independently of δ. We denote by $\mathcal{I}^*(k)$ the set

$$\mathcal{I}^*(k) = \{(w, z, \Delta_{\tilde{q}}) : z = I^*(w; s, \delta, k), |w - k| \le \Delta\}. \tag{3.38}$$

We now consider the inverse image $(\Pi^{\mathrm{p}})^{-1}(\mathcal{I}^*(k)) \subset \mathcal{I}(k)$. By reversing the exchange lemma and considering the dynamics in the regions R_1–R_4 under the reverse flow of (3.36), it is clear that the inverse map $(\Pi^{\mathrm{p}})^{-1}$ applied to $\mathcal{I}^*(k)$ is an $\mathcal{O}(e^{-C/\delta})$ contraction, and its derivatives are also exponentially small. In particular, parametrizing solutions in Σ^{p} by their (w, z)-coordinates, we have that

Copyright © by SIAM. Unauthorized reproduction of this article is prohibited.

$$(\Pi^{\mathrm{p}})^{-1}(w, I^*(w; s, \delta, k)) = (k, z^{\mathrm{p}}(w; s, \delta, k)), \tag{3.39}$$

where the function $z^{\mathrm{p}}(w; s, \delta, k)$ and its derivatives are exponentially small. We now solve for a fixed point of $(\Pi^{\mathrm{p}})^{-1}$, which occurs when $w = k$ and

$$I^*(k; s, \delta, k) = z^{\mathrm{p}}(k; s, \delta, k). \tag{3.40}$$

To solve this equation, we recall from Corollary 2.4 that the manifolds $\mathcal{M}_0^\ell$ and $\mathcal{M}_0^r$ intersect along $\phi_{\mathrm{f}}(k)$ when $s = s^*(k)$, and the distance between $\mathcal{W}^{ss}(\mathcal{M}_0^\ell)$ and $\mathcal{W}^u(\mathcal{M}_0^r)$ in the plane $w = k$ can be represented for small $|s - s^*(k)|$ as

$$D_0(s; k) = M_s(k)(s - s^*(k)) + \mathcal{O}(|s - s^*(k)|^2). \tag{3.41}$$

We note that with Σ^{p} $\mathcal{M}_0^\ell$ is given by the set $z = 0$; we also note that $|z^r(w; s, \delta) - I^*(w; s, \delta, k)| = \mathcal{O}(e^{-C/\delta})$, where the graph of the function $z = z^r(w; s, \delta)$ denotes the intersection of $\mathcal{W}^u(\mathcal{M}_\delta^r)$ with Σ^{p}. Using the distance function (3.41) and the fact that $\mathcal{W}^u(\mathcal{M}_\delta^r)$ is a C^1-$\mathcal{O}(\delta)$ perturbation of $\mathcal{W}^u(\mathcal{M}_0^r)$, we can write

$$z^r(k; s, \delta) = \tilde{M}_s(k)(s - s^*(k)) + \mathcal{O}(\delta, |s - s^*(k)|^2) \tag{3.42}$$

for some $\tilde{M}_s(k) \neq 0$. The matching equation hence becomes

$$\begin{aligned} 0 &= I^*(k; s, \delta, k) - z^{\mathrm{p}}(k; s, \delta, k) \\ &= z^r(k; s, \delta) + \mathcal{O}(e^{-C/\delta}) \\ &= \tilde{M}_s(k)(s - s^*(k)) + \mathcal{O}(\delta, |s - s^*(k)|^2), \end{aligned} \tag{3.43}$$

which can be solved uniquely by the implicit function theorem for $s = s^*(k) + \mathcal{O}(\delta)$, corresponding to a fixed point of the Poincaré map Π^{p} and a periodic orbit close to $\mathcal{P}_0(k)$.

Similar to the proof of Theorem 1.1, by using Proposition 2.2 and undoing the rescalings (2.2), (2.19), we obtain a leading order expression for the wave speed

$$S = \left(\frac{k^2\theta_0^2}{\varepsilon}\right)^{1/3} + \mathcal{O}(1). \tag{3.44}$$

The expression (1.5) for the amplitudes of the periodic orbits follows from the fact that these solutions are obtained as perturbations from the singular limit orbits $\mathcal{P}_0(k)$. Finally, we deduce the statements regarding the periods $T(k, \varepsilon)$ from the fact that the singular orbit $\mathcal{P}_0(a)$ corresponds to the singular homoclinic orbit $\mathcal{H}_0$ and further that the amplitude k of the singular orbit $\mathcal{P}_0(k)$ determines the time spent along the slow manifolds $\mathcal{M}_0^{\ell,r}$ which are of $\mathcal{O}(1/\delta^2)$ and $\mathcal{O}(1/\delta)$, respectively, where we recall that $\delta \sim \varepsilon^{2/3}$. ∎

4. Discussion. In this work, we studied the existence of vegetation stripe pattern solutions of the Klausmeier model (1.1). In particular we found traveling pulses, corresponding to individual vegetation patches as well as periodic wave train solutions, corresponding to repeating vegetation stripe patterns (see Figures 1 and 2 for vegetation stripe profiles obtained via direct numerical simulations). Our results also predict relationships between the speed, amplitude, and wavelength of patterns, and we are able to confirm these using numerical continuation, the results of which are depicted in Figure 8. As predicted by Theorem 1.2, we see that for fixed A, the

Downloaded 05/30/19 to 150.135.174.98. Redistribution subject to SIAM license or copyright; see http://www.siam.org/journals/ojsa.php

Copyright © by SIAM. Unauthorized reproduction of this article is prohibited.

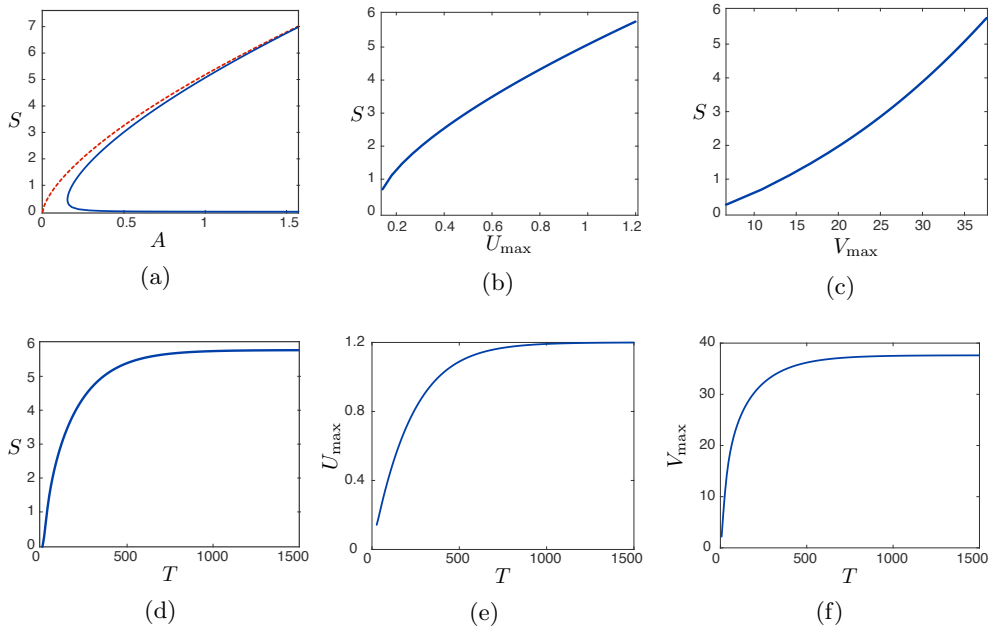

FIG. 8. *Shown are results of numerical continuation for* $m = 0.45$ *and* $\varepsilon = 0.005$ *obtained in AUTO. Panel* (a) *shows how the speed* S *varies with the rainfall* A *for single pulse homoclinic orbits; the blue curve depicts the results of numerical continuation, while the dashed red curve depicts the leading order approximation* $S \approx 5.1915A^{2/3}$ *from Theorem* 1.1. *For fixed* A*, bifurcating from the single pulse homoclinic orbit is a family of periodic orbits corresponding to traveling wave train solutions of* (1.1). *For* $A = 1.2$*, we plot the speed* S *versus the amplitudes* $U_{\max}, V_{\max}$ (b)–(c)*, as well as* S *versus the wavelength* T *of the bifurcating periodic orbits* (d). *Finally* (e)–(f) *depict the amplitudes* $U_{\max}, V_{\max}$ *versus* T.

speed S increases with both amplitude and wavelength, and likewise there is a positive relationship between amplitude and wavelength. The relation between speed and wavelength is in line with empirical observations [4, 8]; we further note that recent empirical observations [4] find a positive relation between biomass and wavelength, and the pattern amplitude $V_{\max}$ serves as one measure of biomass. Also pictured is the relation between the speed S and rainfall A for single pulse homoclinic orbits. We see that this relation forms a C-shaped curve, the upper branch of which closely tracks the leading order approximation given in Theorem 1.1 (shown in dashed red), before turning back along a lower branch of "slow" pulses with smaller wave speeds. While Theorem 1.1 concerns only the upper branch, it is also possible to obtain a detailed understanding of the lower branch of slow pulses using similar techniques, and this is the subject of ongoing work (see also Remark 1.3). We remark that such a C-shaped bifurcation diagram associated with branches of slow and fast pulses has also been observed and studied in detail in other systems such as the FitzHugh–Nagumo model of nerve impulse propagation [5, 6, 7, 18, 26].

Our existence analysis for pulses and wave train solutions is valid in the regime of $A, m = \mathcal{O}(1)$ and $0 < \varepsilon \ll 1$, where (under an appropriate rescaling (2.2)) we are able to capitalize on the slow-fast separation of the traveling wave ODE and employ the methods of geometric singular perturbation theory and blow-up desingularization. In this regime, we find that $\delta = \varepsilon^{2/3}$ is the small parameter which captures the timescale separation. A feature which is immediately apparent from the singular

Copyright © by SIAM. Unauthorized reproduction of this article is prohibited.

Downloaded 05/30/19 to 150.135.174.98. Redistribution subject to SIAM license or copyright; see http://www.siam.org/journals/ojsa.php

Downloaded 05/30/19 to 150.135.174.98. Redistribution subject to SIAM license or copyright; see http://www.siam.org/journals/ojsa.php

perturbation analysis is the inherent degeneracy in the geometry of the traveling wave equation. In particular, in order to rigorously determine the existence of traveling waves, it is necessary to understand the flow near a nonhyperbolic slow manifold as well as slow passage through a degenerate transcritical bifurcation; a somewhat related phenomenon was analyzed in [19]. This degeneracy is responsible for the difficulty in constructing solutions analytically and is also tied to the multitude of scaling regimes needed in order to unfold the bifurcation structure of the traveling wave equation [40].

The present work opens up two main directions of further research. First, there is the question of how our insight into the structure of the three-dimensional existence ODE (1.6)—as governed by (2.4)—is embedded in that of the four-dimensional Gray–Scott type ODE associated to the extended Klausmeier system in which water is allowed to diffuse, i.e., (1.1) with an additional diffusion term $d_W \Delta U$ [35, 41]. Although this specific form is a simplification of the process of water spreading over and/or through soil [15, 43], adding a diffusive effect to the model is crucial for terrains that are gently sloped (or flat). Since water diffuses faster than plants, d_W must be (significantly) larger than 1. In other words, strictly speaking the Klausmeier model (1.1) neglects an effect of at least $\mathcal{O}(1)$. On the other hand, the impact of this effect on the dynamics of traveling patterns seems to be limited on terrains with sufficiently steep slopes. As a first step toward understanding this, one thus has to unravel the way a decreasing diffusivity parameter d_W transforms the geometry of the flow of the four-dimensional ODE as studied in [35, 41] to that of the present three-dimensional "core." This is nontrivial problem, especially since the "classical" four-dimensional Gray–Scott type approach of [10, 11] has been stretched to its limits in [35] and could not be extended beyond a certain critical relation between the diffusion and steepness parameters in the slow U-equation.

Finally, we comment on the stability of the patterns in the underlying PDE (1.1). The direct numerical simulations (see Figures 1 and 2) suggest that the patterns are stable in one spatial dimension. In the setting of the extended generalized Klausmeier–Gray–Scott models, the stability of homoclinic pulses has been established in one space dimension (for certain parameter combinations) [35, 41]. However, in two space dimensions, i.e., as stripe patterns, the constructed homoclinic structures are unstable [35, 41]. This is typically the case for homoclinic stripes in singularly perturbed two-component reaction-diffusion systems considered in the literature; the lateral destabilization is associated to the unstable eigenvalue of the homoclinic solution of the scalar fast reduced equation (the V-equation of (1.1) with $U \equiv \bar{U}$ constant) [12, 25]. Since the pulse structures constructed here are based on a fast heteroclinic jump, there is a reason to expect the associated stripes to be stable. In fact, in [41] stable stripes have been observed in the generalized Klausmeier–Gray–Scott model with $d_W \neq 0$ on sufficiently steep hillsides (beyond the reach of the analysis in [35]).

A complete linear (and nonlinear) stability analysis of the homoclinic and periodic pulses constructed here is outside the scope of this article. In fact, the degenerate bifurcational structure of the Klausmeier model motivates the analysis of a modified Klausmeier model, with additional parameters introduced in order to regularize the equations and unfold these bifurcations more naturally. We refer to [2] for related work in this direction.

REFERENCES

[1] N. Barbier, P. Couteron, and V. Deblauwe, *Case study of self-organized vegetation patterning in dryland regions of central Africa*, in Patterns of Land Degradation in Drylands, Springer, New York, 2014, pp. 347–356.

Copyright © by SIAM. Unauthorized reproduction of this article is prohibited.

[2] R. Bastiaansen, P. Carter, and A. Doelman, *Stable planar vegetation stripe patterns on sloped terrain in dryland ecosystems*, submitted.
[3] R. Bastiaansen and A. Doelman, *The dynamics of disappearing pulses in a singularly perturbed reaction-diffusion system with parameters that vary in time and space*, Phys. D, to appear.
[4] R. Bastiaansen, O. Jaïbi, V. Deblauwe, M. Eppinga, K. Siteur, E. Siero, S. Mermozh, A. Bouveth, A. Doelman, and M. Rietkerk, *Multi-stability of model and real dryland ecosystems through spatial self-organization*, Proc. Natl. Acad. Sci. USA, 115 (2018), pp. 11256–11261.
[5] P. Carter and B. Sandstede, *Fast pulses with oscillatory tails in the FitzHugh–Nagumo system*, SIAM J. Math. Anal., 47 (2015), pp. 3393–3441.
[6] P. Carter and B. Sandstede, *Unpeeling a homoclinic banana in the FitzHugh–Nagumo system*, SIAM J. Appl. Dyn. Syst., 17 (2018), pp. 236–349.
[7] A. R. Champneys, V. Kirk, E. Knobloch, B. E. Oldeman, and J. Sneyd, *When Shil'nikov meets Hopf in excitable systems*, SIAM J. Appl. Dyn. Syst., 6 (2007), pp. 663–693.
[8] V. Deblauwe, P. Couteron, J. Bogaert, and N. Barbier, *Determinants and dynamics of banded vegetation pattern migration in arid climates*, Ecological Monographs, 82 (2012), pp. 3–21.
[9] V. Deblauwe, P. Couteron, O. Lejeune, J. Bogaert, and N. Barbier, *Environmental modulation of self-organized periodic vegetation patterns in sudan*, Ecography, 34 (2011), pp. 990–1001.
[10] A. Doelman, R. A. Gardner, and T. J. Kaper, *Large stable pulse solutions in reaction-diffusion equations*, Indiana Univ. Math. J., 50 (2001), pp. 443–507.
[11] A. Doelman, T. J. Kaper, and P. A. Zegeling, *Pattern formation in the one-dimensional Gray–Scott model*, Nonlinearity, 10 (1997), pp. 523–563.
[12] A. Doelman and H. van der Ploeg, *Homoclinic stripe patterns*, SIAM J. Appl. Dyn. Syst., 1 (2002), pp. 65–104.
[13] A. Doelman and F. Veerman, *An explicit theory for pulses in two component, singularly perturbed, reaction–diffusion equations*, J. Dynam. Differential Equations, 27 (2015), pp. 555–595.
[14] N. Fenichel, *Geometric singular perturbation theory for ordinary differential equations*, J. Differential Equations, 31 (1979), pp. 53–98, https://doi.org/10.1016/0022-0396(79)90152-9.
[15] E. Gilad, J. von Hardenberg, A. Provenzale, M. Shachak, and E. Meron, *Ecosystem engineers: From pattern formation to habitat creation*, Phys. Rev. Lett., 93 (2004), 098105.
[16] K. Gowda, S. Iams, and M. Silber, *Signatures of human impact on self-organized vegetation in the Horn of Africa*, Scientific Reports, 8 (2018).
[17] K. Gowda, H. Riecke, and M. Silber, *Transitions between patterned states in vegetation models for semiarid ecosystems*, Phys. Rev. E, 89 (2014), 022701.
[18] J. Guckenheimer and C. Kuehn, *Homoclinic orbits of the FitzHugh-Nagumo equation: The singular-limit*, Discrete Contin. Dyn. Syst. Ser. S, 2 (2009), pp. 851–872.
[19] M. Holzer and N. Popovic, *Wavetrain solutions of a reaction-diffusion-advection model of mussel-algae interaction*, SIAM J. Appl. Dyn. Syst., 16 (2017), pp. 431–478.
[20] D. Iron, M. Ward, and J. Wei, *The stability of spike solutions to the one-dimensional Gierer-Meinhardt model*, Phys. D, 150 (2001), pp. 25–62.
[21] C. Jones, N. Kopell, and R. Langer, *Construction of the Fitzhugh-Nagumo pulse using differential forms*, in Patterns and Dynamics in Reactive Media, Springer, New York, 1991, pp. 101–115.
[22] C. A. Klausmeier, *Regular and irregular patterns in semiarid vegetation*, Science, 284 (1999), pp. 1826–1828.
[23] T. Kolokolnikov, M. Ward, and J. Wei, *The existence and stability of spike equilibria in the one-dimensional Gray–Scott model: The low feed-rate regime*, Stud. Appl. Math., 115 (2005), pp. 21–71.
[24] T. Kolokolnikov, M. Ward, and J. Wei, *The existence and stability of spike equilibria in the one-dimensional Gray–Scott model: The pulse-splitting regime*, Phys. D, 202 (2005), pp. 258–293.
[25] T. Kolokolnikov, M. Ward, and J. Wei, *Zigzag and breakup instabilities of stripes and rings in the two-dimensional Gray–Scott model*, Stud. Appl. Math., 116 (2006), pp. 35–95.
[26] M. Krupa, B. Sandstede, and P. Szmolyan, *Fast and slow waves in the FitzHugh–Nagumo equation*, J. Differential Equations, 133 (1997), pp. 49–97.
[27] M. Krupa and P. Szmolyan, *Extending geometric singular perturbation theory to nonhyperbolic points—fold and Canard points in two dimensions*, SIAM J. Math. Anal., 33 (2001), pp. 286–314.

Downloaded 05/30/19 to 150.135.174.98. Redistribution subject to SIAM license or copyright; see http://www.siam.org/journals/ojsa.php

Copyright © by SIAM. Unauthorized reproduction of this article is prohibited.

[28] M. Krupa and P. Szmolyan, *Extending slow manifolds near transcritical and pitchfork singularities*, Nonlinearity, 14 (2001), pp. 1473–1491.
[29] M. Krupa and P. Szmolyan, *Relaxation oscillation and canard explosion*, J. Differential Equations, 174 (2001), pp. 312–368.
[30] J. Ludwig, B. Wilcox, D. Breshears, D. Tongway, and A. Imeson, *Vegetation patches and runoff-erosion as interacting ecohydrological processes in semiarid landscapes*, Ecology, 86 (2005), pp. 288–297.
[31] W. Macfadyen, *Vegetation patterns in the semi-desert plains of British Somaliland*, Geographical J., 116 (1950), pp. 199–211.
[32] D. Morgan, A. Doelman, and T. Kaper, *Stationary periodic patterns in the* 1*D Gray–Scott model*, Methods Appl. Anal., 7 (2000), pp. 105–150.
[33] M. Rietkerk, M. Boerlijst, F. van Langevelde, R. HilleRisLambers, J. van de Koppel, L. Kumar, H. Prins, and A. de Roos, *Self-organization of vegetation in arid ecosystems*, American Naturalist, 160 (2002), pp. 524–530.
[34] W. Schlesinger, J. Reynolds, G. Cunningham, L. Huenneke, W. Jarrell, R. Virginia, and W. Whitford, *Biological feedbacks in global desertification*, Science, 247 (1990), pp. 1043–1048.
[35] L. Sewalt and A. Doelman, *Spatially periodic multipulse patterns in a generalized Klausmeier–Gray–Scott model*, SIAM J. Appl. Dyn. Syst., 16 (2017), pp. 1113–1163.
[36] J. A. Sherratt, *Pattern solutions of the Klausmeier model for banded vegetation in semi-arid environments* I, Nonlinearity, 23 (2010), pp. 2657–2675.
[37] J. A. Sherratt, *Pattern solutions of the Klausmeier model for banded vegetation in semi-arid environments* II: *Patterns with the largest possible propagation speeds*, Proc. A, 467 (2011), pp. 3272–3294.
[38] J. A. Sherratt, *Pattern solutions of the Klausmeier model for banded vegetation in semi-arid environments* III: *The transition between homoclinic solutions*, Phys. D, 242 (2013), pp. 30–41.
[39] J. A. Sherratt, *Pattern solutions of the Klausmeier model for banded vegetation in semiarid environments* IV: *Slowly moving patterns and their stability*, SIAM J. Appl. Math., 73 (2013), pp. 330–350.
[40] J. A. Sherratt, *Pattern solutions of the Klausmeier model for banded vegetation in semiarid environments* V: *The transition from patterns to desert*, SIAM J. Appl. Math., 73 (2013), pp. 1347–1367.
[41] E. Siero, A. Doelman, M. B. Eppinga, J. D. M. Rademacher, M. Rietkerk, and K. Siteur, *Striped pattern selection by advective reaction-diffusion systems: Resilience of banded vegetation on slopes*, Chaos, 25 (2015), 036411.
[42] C. Valentin, J. d'Herbès, and J. Poesen, *Soil and water components of banded vegetation patterns*, Catena, 37 (1999), pp. 1–24.
[43] S. van der Stelt, A. Doelman, G. Hek, and J. Rademacher, *Rise and fall of periodic patterns for a generalized Klausmeier–Gray–Scott model*, J. Nonlinear Sci., 23 (2013), pp. 39–95.
[44] J. von Hardenberg, E. Meron, M. Shachak, and Y. Zarmi, *Diversity of vegetation patterns and desertification*, Phys. Rev. Lett., 87 (2001), 198101.
[45] B. Wilcox, D. Breshears, and C. Allen, *Ecohydrology of a resource-conserving semiarid woodland: effects of scale and disturbance*, Ecological Monographs, 73 (2003), pp. 223–239.

Downloaded 05/30/19 to 150.135.174.98. Redistribution subject to SIAM license or copyright; see http://www.siam.org/journals/ojsa.php

Copyright © by SIAM. Unauthorized reproduction of this article is prohibited.